GMR
The Original

BIOGENIC ZINC OXIDE NANOPARTICLE FABRICATION USING *KIGELIA PINNATA* AQUEOUS LEAF EXTRACT AND ITS CHARACTERISATION, ANTIOXIDANT AND ANTICANCER EVALUATION

Priyanaka V[1], Raveesha H. R[2]*

[1,2]Department of Botany, Jnanabharathi Campus, Bangalore University, Bengaluru – 560056, Karnataka, India
Emails: raveesha74@bub.ernet.in[1]; hrraveesh74@gmail.cm[2]
[2]Orcid: https://orcid.org/0000-0001-9880-1805

ABSTRACT
Kigelia pinnata, commonly known as sausage tree, belongs to the Bignoniaceae family and is a medicinal plant rich in flavonoids, iridoids, and naphthoquinones. The present study deals with aqueous leaf extract to biofabricate zinc oxide nanoparticles (ZnO NPs). The synthesised nanoparticles were characterised for their morphology, size and properties using different analytical techniques like UV-Vis spectroscopy, XRD, FTIR, SEM-EDAX, HR-TEM, DLS and Zeta potential. The synthesised nanoparticles were crystalline, ultra-small (4-8 nm by HR TEM) and moderately stable (-20.4 mV). They exhibited potent antioxidant activity with ABTS and DPPH IC_{50} values (4.49 and 4.81 µg/mL) comparable to ascorbic acid, and higher ferric-reducing efficiency (FRAP IC_{50} - 15.07 µg/mL). Photocatalytic assays confirmed effective methylene blue degradation (58.81 % in 180 min). Cytotoxicity tests showed selective anticancer activity, most potent against HCT-116 cells with an IC_{50} value of 39.39 µg/mL, including apoptosis, ROS generation, caspase-3 activation, and G2/M arrest. Overall, *K. pinnata*-mediated ZnO NPs show promise as eco-friendly nanomaterials with biomedical and environmental applications.

KEYWORDS: *Kigelia pinnata*, ABTS, Cytotoxicity, IC_{50}, HCT-116, nanoparticles

1. INTRODUCTION

Nanomaterials have a wide spectrum of applications due to their morphology and size, and have been an essential subject in the fields of basic and applied sciences. Recently, there has been a significant focus on nano-sized semiconductors because of their novel properties, which have applications in optoelectronics. Among various nanoparticles, zinc oxide nanoparticles (ZNPs) are promising semiconductors that display significant optical transparency and luminescent properties in UV–Visible (UV–Vis) regions (Cao et al. 2011). Zinc oxide (ZnO) nanoparticles are widely explored for their multifunctional utilisation in biomedicine, catalysis, and environmental remediation due to their photocatalytic efficiency, biocompatibility, and reactive surface chemistry (Rasmussen *et al.* 2010). The chemical nanoparticle synthesis methods involve many poisonous chemicals that negatively impact the environment and health (Iravani, 2011). To overcome this, green synthesis of nanoparticles using plant extracts is environmentally friendly. The phytochemicals present in the plants act as natural reducing and capping agents, stabilising the nanoparticles.

Kigelia pinnata, commonly known as the sausage tree, is a medicinal plant belonging to Bignoniaceae family with reported antioxidant, antimicrobial, and anticancer properties (Hoµghton, 2002). Phytochemicals such as flavonoids, iridoids, and naphthoquinones present in its leaves and fruits are known to facilitate nanoparticle synthesis (Ramadan *et al.* 2022). Earlier reports have illustrated the biosynthesis of silver and copper nanoparticles using *K. pinnata* or *K. africana* extracts, confirming its bioreductive potential (Ashishie *et al.* 2018; Kalainila *et al.* 2015).

Despite these findings, the green synthesis of ZnO nanoparticles using *K. pinnata* leaf extract remains underexplored. ZnO NPs are particularly valuable for biomedical use due to their inherent cytotoxicity against cancer cells and vigorous free-radical scavenging activity (Premanathan *et al.* 2011). This study aims to synthesise ZnO nanoparticles using *K. pinnata* leaf extract and evaluate their properties throµgh UV–Vis, FTIR, XRD, SEM-EDAX, HR-TEM, Zeta potential, and DLS analysis. Further, we evaluated their antioxidant activity (DPPH, ABTS, FRAP) and anticancer efficacy (MTT, Annexin V/PI, cell cycle, ROS expression, caspase-3 expression studies).

MATERIALSAND METHODS PLANT

2. 1. Preparation of *Kigelia pinnata* Leaf Extract

Fresh leaves of *Kigelia pinnata* were collected, thoroughly rinsed with distilled water, and shade-dried for several days until all moisture was eliminated. We then finely powdered the dried material using a mechanical grinder. We boiled ten grams of this powder with 100 mL of distilled water for 30 minutes, filtered the extract using Whatman No. 1 filter paper, and stored it at 4 °C for further experiments.

Fig. 1: Habit of *Kigelia pinnata*

2.2. Synthesis of Zinc Oxide Nanoparticles (ZnONPs)

ZnONPs were synthesised by mixing 50 mL of 0.01 M zinc nitrate solution with 10 mL of the prepared *K. pinnata* leaf extract. The solution was stirred constantly at 60–70 °C for 2 hours. A visible colour change indicated the formation of nanoparticles. The resulting white precipitate was centrifµged at 8000 rpm, washed with distilled water and ethanol, and oven-dried at 60 °C.

2.3. Characterisation Techniques

2.3.1. Chemical and instrumental

All the chemicals and solvents were purchased from Merck (Germany). UV–Visible (UV.1800, Shimadzu, Japan); FT-IR (100 Spectrum, Perkin Elmer, Germany); XRD (EQUINX 3000; Intel, France); FESEM (ZIGMAVP-500, Zeiss, Germany; EDS, Oxford instruments, UK); Ultra sonic (S15H, Germany); Heater-Stirrer (MR Hei-End, Germany); Oven (Memmert 100-800, Germany); Rotary evaporator (4003 Heidolph, Germany); Centrifµge (EBA 20 Hettich, Germany); JSM-JEOL 6390.

2.3.2. UV–Vis Spectroscopy: 1 mL of the suspension was collected from the purified sample at the end of the reaction and was sonicated at 4000 rpm for 15 min. Absorbance spectra (200–800 nm) were recorded to confirm nanoparticle formation, followed by the method as per Fakhari *et al.* (2019), with slight modifications.

2.3.3. Fourier Transform Infrared Spectroscopy (FTIR): ZnONPs aqueous leaf extract of *Kigelia pinnata* was carried out by the KBr pellet method to identify functional groups in the extract responsible for reduction and capping of ZnONPs, and the presence of the various vibrational modes in the synthesised nanoparticles was investigated, followed by the method as per Fakhari *et al.* (2019), with slight modifications.

2.3.4. X-ray Diffraction (XRD): The X-ray peak profile analysis (XPPA) was utilized to obtain the crystallite size, lattice parameters, lattice strain, lattice stress and strain energy density [18] using D8 Advance diffractometer (Bruker, Germany) with Cu-Kα radiation (λ = 0.15406 nm) at an accelerating voltage of 40 kV with an emission current of 30 mA.Crystalline structure was examined, and average crystallite size was calculated using Debye-Scherrer's formula Ismail *et al.*2018.

2.3.5. Scanning Electron Microscopy (SEM) & EDAX: To determine morphology and elemental composition. Scanning Electron Microscopy (SEM) images of the zinc oxide nanoparticles were obtained using a JSM-JEOL 6390 Scanning Electron Microscope. The JSM-6390 is a high-performance, low-cost scanning electron microscope with a high resolution of 3nm. The instrument features a user-friendly graphical interface that enables easy operation.

It also comes with an automatic coater for sample preparation, which adjusts the coating duration on its own.; it varies according to the nature of the sample described by Mohan and Ranjanadevi (2016).

2.3.6. High-Resolution Transmission Electron Microscopy (HR-TEM): *K. pinnata* leaf extract was prepared by the hanging drop method with the ZnNPs solution onto the glass slide. The slide was air-dried at room temperature before being analyzed using AFM. The size and surface morphology of ZnNPs were determined by high-resolution transmission electron microscopy (HR-TEM), Daphedar and TC Taranath (2018).

2.3.7. Dynamic Light Scattering (DLS) & Zeta Potential: To analyse particle size distribution and colloidal stability. For dynamic light scattering measurements, a 12 mm cell (DTS 0012) was used. One millilitre of distilled water (or ethylene glycol) was added to the cell, and then 50 µl from stock dispersions was added. Samples were again sonicated for 5 minutes. The nanoparticle size distribution was analyzed using the DLS technique with a Malvern Zetasizer Nano ZS (Malvern Instruments Ltd., UK). The suitable parameters (viscosity, absorption and refractive index) were chosen for each ZnO and dispersant. For ZnO sample: absorption 0.1, refractive index 2.0, for water: viscosity 1.0031cP, refractive index 1.33, ethylene glycol viscosity 1.98 cP, refractive index 1.44. The pH value of each suspension was adjusted by adding NaOH or HCl. Marsalek, R. (2014) recorded histograms with the distributions of sizes.

2.4. Photocatalytic activity

The photocatalytic studies of the leaf extract of *Kigelia pinnata* were done using ZnO NPs as a semiconductor photocatalyst and MB dye as the model dye. The method is followed by Vasundhara *et al.*(2023) with slight modifications. The photocatalytic activity of ZnO NPs was analysed based on the observation of degradation (decolouration) of MB dye. The photocatalytic efficiency was determined using the following equations: $[A0 - A/A0] \times 100$ or $[C0 - C/C0] \times 100$ where $A0$ and A is the initial (0 minute) and final (90 minute) absorbance values of the MB solution without and with ZnO semiconductor photocatalyst and $C0$ and C are the 0 minute and 90 minute MB dye concentrations without and with ZnO semiconductor photocatalyst at 0 minute and 90 minutes respectively.

2.5. Antioxidant Activity

2.5.1. *In vitro* Antioxidant Activity by DPPH Radical Scavenging Assay

The DPPH (2,2-diphenyl-picryl hydrazyl) free radical scavenging assay of ZnONPs aqueous leaf extract of *Kigelia pinnata* was determined as per RajKumar *et al*. (2011) with slight modifications. Various concentrations of leaf extract (3.125, 6.25, 12.50, 25, 50, 100 µg/ml) were mixed with freshly prepared 100 µM of DPPH in different test tubes to achieve the final volume of 1ml. Moreover, the test tubes were kept at 25°C for 15 min. in the dark condition. Following incubation, absorbance was recorded at 517 nm using a semi-automatic analyzer, with the control serving as reference. 80% methanol without the extract in the reaction mixture served as blank, and Ascorbic acid was used as reference standard. IC_{50} value was calculated from the linear or logarithmic regression equation (Y=mx+C) derived from the % DPPH inhibition graph. The % radical scavenging activity of the given compound was calculated using the following formula:

% DPPH Radical Scavenging Activity= [(Abs of Control-Abs of Sample)/Abs of Control] × 100

2.5.2. *In vitro* Antioxidant Activity by ABTS Radical Scavenging Assay

The ABTS (2,2'-azinobis(3-ethylbenzothiazoline-6-sulfonic acid)) free radical scavenging activity of ZnONPs aqueous leaf extract of *Kigelia pinnata* was performed as per Auddy *et al.*(2003) with slight modifications. 10 ml of ABTS (7Mm) and 10 ml of Ammonium per sulfate (2.45 mM) solutions were mixed and incubated at room temperature in the dark for 16 hrs. Thus, the solution is further diluted with phosphate-buffered saline to absorb 1.000 at 734nm. A new ABTS solution was prepared for every assay. Various concentrations of extract (3.125, 6.25, 12.50, 25, 50, 100 µg/ml) were allowed to react with 1ml of the ABTS solution, and the reaction mixture was allowed to incubate for 10 min. in the dark; later, absorbance was taken at 734 nm using a spectrophotometer. The ABTS radical scavenging activity of the extract was evaluated in comparison to the ascorbic acid standard and a control reaction was carried out without the test sample. The percentage inhibition of the ABTS radical scavenging assay was calculated by using the following formula, and the IC_{50} value was calculated using GraphPad Prism software. The % radical scavenging activity of the given compound was calculated using the following formula:

% ABTS Radical Scavenging Activity= [(Abs of Control-Abs of Sample)/Abs of Control] × 100

2.5.3. *In vitro* Antioxidant Activity by FRAP Radical Scavenging Assay

This method is based on the ability of the sample to reduce Fe3+ to Fe2+ ions. At low pH, in the presence of TPTZ (Sigma Aldrich, India), ferric-tripyridyltriazine (Fe3+ -TPTZ) complex is reduced to the ferrous (Fe2+ -TPTZ) form with the formation of an intense blue colour having an absorption maximum at 593 nm. The method described by Benzie and Strain (1996) was followed. 2.3mL of the FRAP reagent was mixed with 0.7 mL of ZnONPs aqueous leaf extract of *Kigelia pinnata* at different concentrations (3.125, 6.25, 12.50, 25, 50, 100 µg/ml). The mixture was then incubated at 37ºC for 30 min in the dark. The absorbance was measured at 593 nm against a blank with all the reagents, excluding the sample, using a spectrophotometer (Systronics Visiscan 167). Increased absorbance of the reaction mixture indicates an increase in reduction capability. Samples were measured in triplicate. Ascorbic acid (Merck, India) was used as the standard with different concentrations. The standard curve of ascorbic acid solution was prepared using a similar procedure from which the regression formula was derived. Results were expressed in mg of ascorbic acid equivalents (AAE)/mL of extract.

Anticancer Activity Maintenance of Cell Line:

The A549 (Human alveolar lung adenocarcinoma cell line) was procured from NCCS, Pune, India. The cells were maintained in Ham's F12k media supplemented with 10 % FBS along with the 1% antibiotic-antimycotic solution in an atmosphere of 5% CO2, 18-20% O2 at 37°C temperature in the CO2 incubator and sub-cultured every 2 days. The passage number of A549 cells was used for the present study.

The HCT-116 (Human colorectal adenocarcinoma cell line) and MCF7 (Human breast adenocarcinoma cell line) were purchased from NCCS, Pune, India. The cells were maintained in DMEM with high glucose media supplemented with 10 % FBS along with the 1% antibiotic-antimycotic solution in an atmosphere of 5% CO2, 18-20% O2 at 37°C temperature in the CO2 incubator and sub-cultured every 2 days. Passage numbers of HCT-116 and MCF7 cells were P71 and P63, respectively, and were used for the present study.

After reaching 80% density, cells were detached using 0.025% trypsin and 0.01% EDTA (in D-PBS) solution. Cell viability and count were performed using a hemocytometer.

The appropriate density of cells was seeded in T25 flasks and cultured until further usage.

2.6.1. Cell viability and proliferation studies - MTT assay:

The cytotoxicity effect of ZnONPs aqueous leaf extract of *K. pinnata* was analysed on A549, HCT-116 and MCF7 cells by performing the MTT assay as per Mosmann (1983) with slight modifications. MTT is a tetrazolium salt converted into insoluble purple-colored formazan crystals by the action of the lactate dehydrogenase enzyme released by mitochondria. Cells in 200µl of suitable media and at a density of 10,000 were plated in a 96-well plate and incubated at 37°C overnight. After attachment of cells to the surface of the cell culture plate, the spent medium was replaced with complete media having different concentrations of *K. pinnata* leaf extract (12.5, 25, 50, 100 and 200µg/mL). After the addition of the drµg, cells were incubated for 24 hours. at 37°C with 5% CO2 atmosphere. After incubation, cells were treated with 100µL of MTT (0.5 mg/mL) and incubated for 3 hours. at 37°C. DMSO (100µL) was used to dissolve the formazan crystals, and the purple colour was measured at 570 nm using a microplate reader (ELX-800, BioTek, USA). The viability of cells treated with DMEM alone was considered as 100%. % cell viability is calculated using the following formula:

% cell viability = [OD of treated cells/OD of Untreated cells] * 100

The IC50 value was determined using a linear regression equation, i.e. Y =Mx+C. Y = 50, M and C values were derived from the viability graph.

Cell morphological assessment:

Morphological changes in A549, HCT-116 and MCF7 cells were assessed after post-treatment with a ZnONPs aqueous leaf extract of *Kigelia pinnata* with concentrations ranging from 12.5µg/ml to 200µg/ml for 24 hours. at 37°C. Cells were observed and recorded using an Inverted Biological Microscope (CKX-41, Olympus) with a camera's help and recorded using MICAM software at 20x magnification. Scale: 200uM.

2.6.2. Apoptosis/Necrosis study by Flow Cytometry: Annexin V/PI staining

After treatment, the culture medium was removed, and cells were rinsed once with phosphate-buffered saline (PBS). Each well then received 500 µl of trypsin-EDTA and was incubated at 37°C for 3–4 minutes to facilitate cell detachment. Detachment was halted by adding 2 ml of complete culture medium, and cells were transferred into 12 × 75 mm polystyrene tubes. Cell suspensions were centrifµged at 300 × g for 5 minutes at room temperature (25°C). The supernatant was discarded, and the cell pellets were washed twice with PBS. After removing the wash buffer completely, cells were resuspended in 100 µl of Annexin V binding buffer containing 5 µl of FITC-conjµgated Annexin V. The samples were gently mixed and incubated in the dark at room temperature for 15 minutes. Following incubation, 5 µl of propidium iodide (PI) was added, along with 400 µl of 1× binding buffer. Tubes were gently vortexed and immediately processed for flow cytometric analysis. Samples were analysed using a BD FACSCalibur™ flow cytometer. Data acquisition was initiated promptly after PI addition, and at least 10,000 events were collected per sample. The data were analysed using BD CellQuest Pro software (version 2.0).

2.6.3. ROS expression study by Flow Cytometry: H2DCFDA staining

Cells were seeded in 6-well plates at a density of 0.5×10^6 cells per well in 2 ml of complete medium and incubated overnight at 37°C in a humidified CO_2 incubator. After 24 hours, the medium was aspirated, and cells were rinsed once with 1 ml of 1× PBS. Cells were then treated with various concentrations of zinc oxide nanoparticles (ZnONPs) synthesised from aqueous leaf extract of *Kigelia pinnata*. An untreated control group was included. Treatments were applied in 1 ml of fresh medium and incubated for 24 hours under the same conditions. Following treatment, culture supernatants were transferred into labelled 12 × 75 mm polystyrene tubes. Cells were washed with 500 µl PBS, which was added to the same tubes. After removing PBS, 500 µl of trypsin-EDTA was added to each well, and cells were incubated at 37°C for 3–4 minutes. The collected media were returned to the wells to neutralise trypsin, and the detached cells were transferred into their corresponding tubes. Samples were centrifµged at 300 × g for 5 minutes at room temperature. Supernatants were discarded, and pellets were washed twice with PBS, followed by complete removal of residual buffer. For ROS detection, a 10 µM working solution of H_2DCFDA (prepared by diluting a 4 mM stock in DMSO with DPBS) was used. Cells were resuspended in this solution at a density of 1×10^6 cells/ml and incubated at 37°C for 30 minutes in the dark. After staining, cells were centrifµged at 150 × g for 5 minutes, and the supernatant was discarded. Pellets were

gently resuspended in 400 µl of pre-warmed DPBS. Fluorescence was measured immediately using a BD FACSCalibur™ flow cytometer (excitation: 488 nm; emission: 535 nm, FL1 channel). A minimum of 10,000 events was acquired per sample. Data analysis was performed using BD CellQuest Pro software (v2.0). The procedure was adapted from Eruslanov and Kusmartsev (2009) with minor modifications.

2.6.4. Caspase-3 expression study by Flow Cytometry:

This assay was performed with minor modifications based on the method described by Belloc *et al*. (2000). Cells were seeded into 6-well plates at a density of 0.5×10^6 cells per well in 2 ml of complete medium and incubated overnight at 37°C in a humidified CO_2 incubator. After 24 hours, the medium was removed and cells were gently rinsed with 1 ml of 1× PBS. Cells were then treated with various concentrations of zinc oxide nanoparticles (ZnONPs) synthesised from aqueous leaf extract of *Kigelia pinnata*, while untreated cells served as the control. Treatments were administered in 1 ml of fresh medium and incubated for another 24 hours. Post-treatment, the medium from each well was collected into labelled 12 × 75 mm polystyrene tubes. Cells were washed with 500 µl PBS, which was also added to the respective tubes. After aspirating the PBS, 500 µl of trypsin-EDTA was added to each well and incubated at 37°C for 3–4 minutes. The collected medium was then returned to neutralise the trypsin, and the detached cells were transferred into the same tubes. Cells were centrifµged at 300 × g for 5 minutes at 25°C, and the supernatant was discarded. Pellets were washed twice with PBS and resuspended in 1 ml of cold 70% ethanol, added dropwise while vortexing to ensure even fixation and minimise clumping. Fixed cells were incubated at –20°C for 30 minutes. After incubation, cells were pelleted by centrifµgation at a higher speed, and the ethanol was carefully removed. Pellets were resuspended in 20 µl of FITC-conjµgated anti-caspase-3 antibody, mixed gently, and incubated for 30 minutes at room temperature (20–25°C) in the dark. Samples were then washed with 1× PBS containing 0.1% sodium azide and resuspended in 0.5 ml PBS. Flow cytometric analysis was performed using a BD FACSCalibur™ flow cytometer with excitation at 488 nm and emission detection at 535 nm (FL1 channel). If not analysed immediately, samples were mixed thoroµghly before acquisition. At least 10,000 events were recorded per sample, and data were analysed using BD CellQuest Pro software (version 2.0).

RESULTS AND DISCUSSION

1.1. Characterisation of Phytofabricated Zinc Oxide Nanoparticles (ZnO NPs)

1.1.1. UV- Vis spectroscopic analysis

The first visual confirmation of nanoparticle synthesis was the formation of a pale white suspension (Fig. 2) on adding the reaction mixtures, indicating that the phytochemicals in the aqueous leaf extract had reduced the zinc nitrate. These observations confirm earlier reports by Ogunyemi *et al.*(2019), who made a similar observation on synthesising ZnO NPs using three different plant extracts.

Fig. 3 shows the UV-Vis absorption spectra. The 200-800 nm wavelength spectrum shows a clear absorption range typical for ZnO NPs. The synthesised NPs dissolved in DMSO showed maximum absorption at 250 nm, with absorbance values of 2.497 for the synthesised form and 2.979 for the purified form. A sharp absorption peak appeared at 268 nm, characteristic of green-synthesised ZnO NPs, indicating successful biofabrication of ultra-small ZnO NPs (Zhang *et al.* 2013). This peak corresponds to the intrinsic band gap absorption of ZnO nanoparticles, which results from the movement of electrons from the valence band into the conduction band (Rud *et al.* 2023). Generally, for ZnO the band gap is ~3.37 eV, corresponding to an absorption peak at 370-390 nm (Look, 2001), in the present study the phytofabricated ZnO NPs absorb slightly shorter wavelength, indicating a blue shift due to the bioreduction and capping by phytochemical present the leaves of *K. pinnata* (Iravani, 2011). Higher absorption in the purified NPs shows better dispersion and optical purity (Rajkumar *et al.* 2013). Recent studies of the Phytofabrication of ZnO NPs have reported similar findings. Udayagiri *et al.* (2024) observed an absorption peak at 360-370 nm, linked to small, well-dispersed, spherical particles. Tiwari *et al.* (2024) confirmed strong UV absorption and band-edge features in ZnO NPs synthesised using plant extracts. Subramanian *et al.* (2024) reported that phytofabrication maintains nanocrystalline size (~18 nm) and optical clarity, with characteristic UV absorption indicating uniform morphology and minimal impurities.

a. Reaction mixture b. Synthesised ZnO NPs

Fig. 2: Synthesised zinc nanoparticles solution and precipitated ZnO NPs

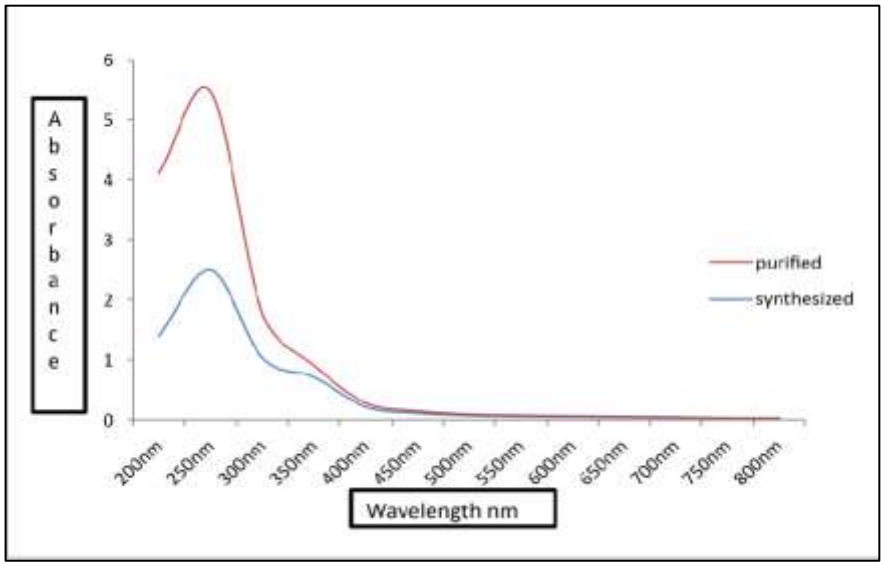

Fig. 3: UV-visible absorption spectrum of the synthesised and DMSO-purified ZnO NPs of *K. pinnata* leaf.

1.1.2. FTIR spectroscopic analysis

To identify the functional groups present in the *K. pinnata* leaf-mediated ZnO NPs, FTIR spectroscopy was used, which confirms the role of biomolecules in NPs formation and the Zn-O bond formation. A sharp peak was observed at 770 cm^{-1} and 585 cm^{-1} (Fig.4), corresponding to Zn-O binding, verifying a successful formation of ZnO NPs (Rajkumar & Rahuman, 2011). The absorption band at 3281 cm^{-1} relates to the O-H stretching vibrations, specifying the presence of hydroxyl groups, possibly from phenolic compounds, flavonoids or water molecules in the aqueous leaf extract. The peaks at 2980 cm^{-1}, 2852 cm^{-1}, and 1531 cm^{-1} correspond to alkanes and amine salts, which might be derived from proteins and alkaloids in the plant extract (Almed *et al.* 2016). The bands at 1726 cm^{-1}, 1633 cm^{-1} might be associated with carbonyl groups and alkenes, indicating the presence of flavonoids and other unsaturated biopolymers (Song & Kim, 2009). The bands at 1242 cm^{-1} and 1029 cm^{-1} in the ZnO NPs were due to the aliphatic amines and alcohols, which are part of phytochemicals. The observed peaks at 664 cm^{-1} and 625 cm^{-1} are associated with the halo compounds, which are less commonly seen in NPs but are undoubtedly present in the secondary metabolites. These functional groups are key in reducing the zinc ions and stabilising the NPs by surface functionalization. These absorption peaks support the green synthesis method and prove the use of plant samples as a sustainable, effective and environmentally friendly NPs production.

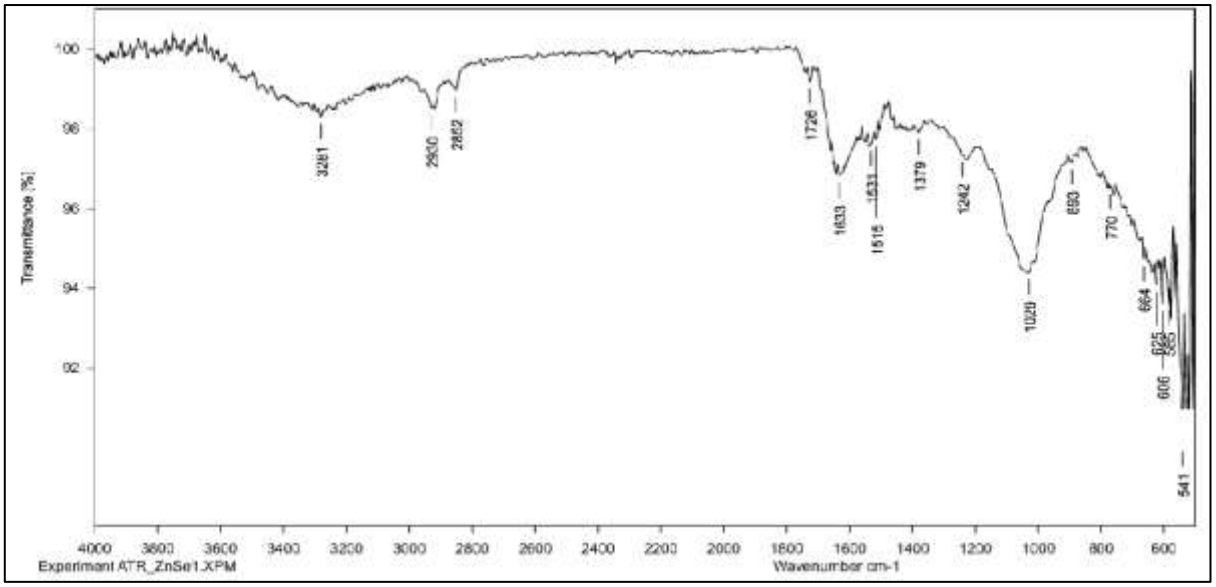

Fig. 4: FTIR absorption spectrum of ZnO NPs of *K. pinnata* leaf.

The FTIR results are confirmed by earlier reports by various researchers on phytofabricated ZnO NPs. Ramesh *et al.* (2024) showed that ZnO stretching vibrations in the FTIR spectrum are a definitive marker of ZnO NPs formation in plant extract-mediated synthesis. In the present work, firm absorption peaks at 770 cm^{-1} and 585 cm^{-1} support the formation of ZnO bonds. Patel *et al.* (2024) reported that O-H stretching bands around 3280 cm^{-1} originate from the phenolic and flavonoid compounds, which are likely to be present in the aqueous leaf extract of *K. pinnata*, which acts as a natural stabilising and capping agent. The C-H and amine peaks at 2980 cm^{-1}, 2852 cm^{-1} and 1531 cm^{-1} are associated with plant proteins and alkaloids, which support nanoparticle capping (Das *et al.* 2023).

1.1.3. X-ray diffraction (XRD) Analysis

The crystallite nature and the average size of the particles were estimated using X-ray diffraction analysis. Fig. 5 shows the XRD pattern of ZnO NPs. X-ray diffraction pattern for the green synthesised ZnO NPs reveals a distinct diffraction peak at $2\theta = 39.2°$, corresponding to the (101) crystalline plane of hexagonal wurtzite ZnO. It validates the crystalline nature of the NPs. As per the JCPDS card no. 36-1451, the major diffraction peaks for wurtzite ZnO are observed at (100) → ~31.7°; (002) → ~34.4°; (101) → ~36.2°; (102), (110), (103), (112)
(Borker & Salker, 2006). The slight shift to 39.2° may be due to lattice strain or defect-induced stress from phytochemicals. The surface adsorption of phytochemicals slightly distorts the ZnO crystal lattice (Gunalan *et al.* 2012; Iravani, 2011). The smaller and less intense peaks correspond to background noise or the fractional impurities in the sample.
Using Scherrer's equation, the average crystallite size was calculated (Patterson, 1939), and it was found to be approximately 39.1 nm, indicating nanoscale domains for the synthesised ZnO NPs. These findings align with the previously reported biosynthesised ZnO NPs in the 20-50 nm range (Gunalan *et al.* 2012).

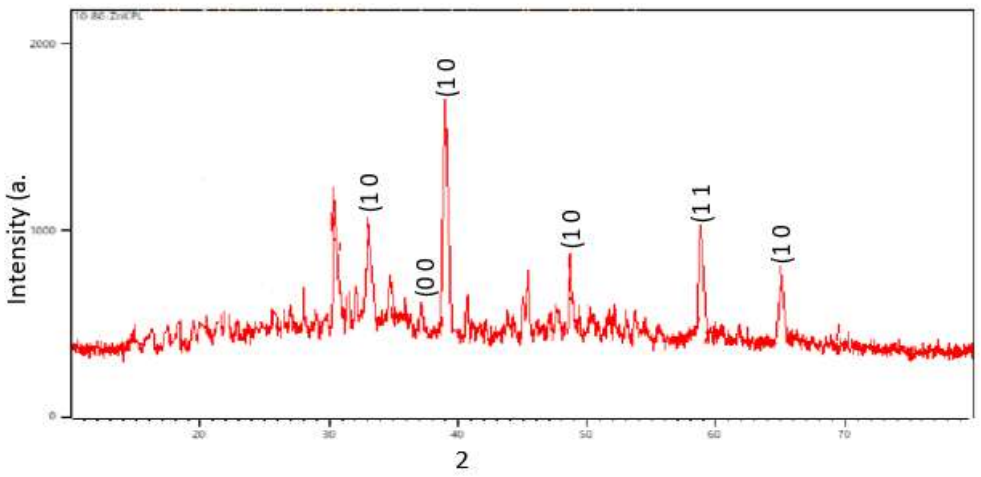

Fig.5: X-ray diffraction (XRD) pattern of ZnO NPs of *K. pinnata* leaf.

Borker and Salker (2006) reported the characteristic diffraction peaks of wurtzite ZnO typically appearing at 2θ values near 31.7°, 34.4°, and 36.2° for the (100), (002), and (101) planes, respectively. The prominent (101) plane peak, which appeared slightly shifted to 39.2^0 in the
present study, sμggests lattice strain or defect-induced stress, which occurs as the phytochemicals adsorb to the nanoparticle surface during green synthesis (Gunalan et al. 2012; Iravani, 2011).

1.1.4. Scanning Electron Microscopy and EDAX analysis

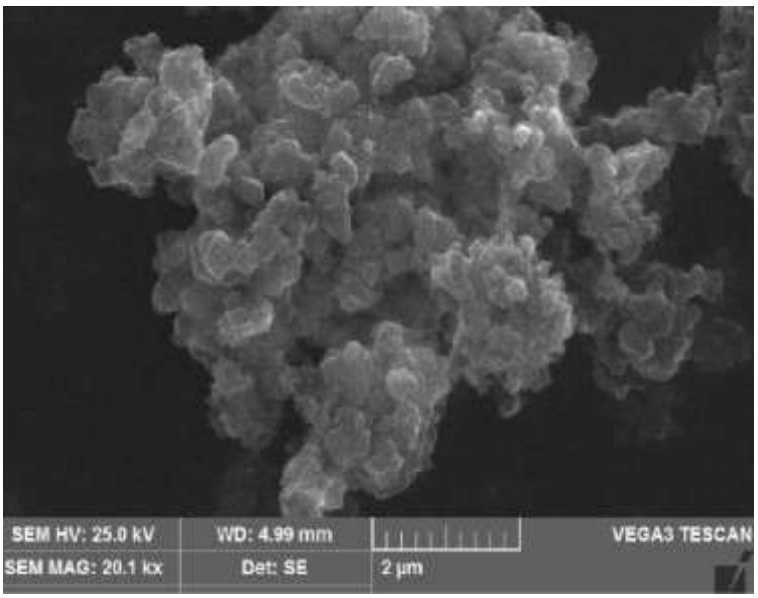

Fig. 6: SEM micrographs of ZnO NPs of *K. pinnata* leaf.

The SEM analysis was carried out on the green-synthesised ZnO NPs to study the morphology and determine the size of the particles. The SEM micrographs (Fig. 6) reveal agglomerated and clustered particles, common in plant-mediated green-synthesised NPs due to residual biomolecules on the surface. They are roμghly spherical to irregular in shape, sμggesting it is anisotropic growth under ambient synthesis conditions. These aggregates exhibit a porous surface, suitable for catalytic and biomedical applications. The particle size ranges from 50 to 200 nm, specifying the nanocrytalline ZnO clusters (Kharissova *et al.* 2019).
Further, the firm peaks for zinc (Zn) and oxygen (O) from the Energy-Dispersive X-ray spectroscopy confirm the elemental identity of the synthesised material as ZnO (Fig. 7). Moreover, the absence of other significant elemental peaks implies a high purity of the ZnO NPs. The Zn/O ratio is moderately skewed due to surface oxygen adsorption or overlapping signals (Sharma *et al.* 2004). These data affirmatively support the efficiency of *K. pinnata* leaf extract as a natural bioreductant and stabilising agent in the phytofabrication of ZnO NPs.

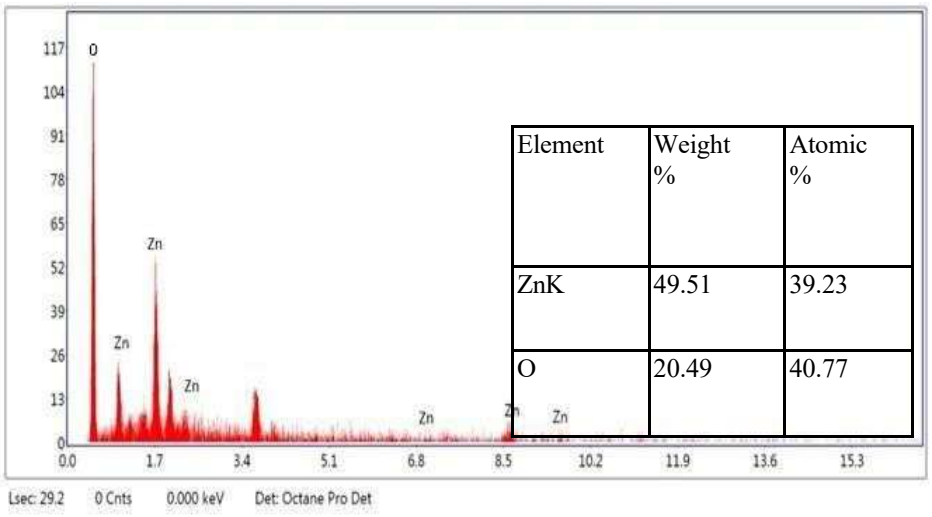

Element	Weight %	Atomic %
ZnK	49.51	39.23
O	20.49	40.77

Fig. 7: EDAX spectrum of ZnO NPs of *K. pinnata* leaf

As reported by Patel *et al.* (2024), the porous agglomerates can enhance surface area, making them valuable for catalytic and biomedical uses. The slight deviation in the Zn/O ratio can be attributed to the surface oxygen adsorption, characteristic of phytofabricated ZnO NPs (Das *et al.* 2023)

1.1.5. HR-TEM analysis

The HR-TEM micrographs (Fig. 8) at different scales (200 nm to 5 nm) reveal high-resolution insights into the shape, dispersion and internal structure of the biosynthesised ZnO NPs. At a lower magnification of 200 nm (Fig. 8-a), ZnO NPs appear aggregated into larger clusters, standard in green-synthesised NPs due to plant residual stabilising agents. At a higher magnification of 100 nm (Fig. 8-b), the particle distribution gets clearer, exhibiting well-defined, more dispersed NPs. Magnification of 50 nm (Fig. 8-c) reveals densely packed, almost spherical NPs, sµggesting a higher nucleation rate during synthesis. At a 20 nm (Fig. 8-d) scale, the primary particle size is measured to be 4 nm and 8 nm, confirming the formation of ultra-small NPs. The structural details are visible at 5 nm magnification (Fig. 8-e), where lattice fringes become visible. The presence of lattice fringes supports the nanocrystalline nature of the particles, with internal ordering characteristic of hexagonal wurtzite ZnO (Wang, 2004; Ali *et al.* 2021). Hence, the HR-TEM micrographs confirm the successful phyto fabrication of highly crystalline, well-dispersed ZnO NPs with a primary particle size ranging from 4-8 nm. Similarly, Singh *et al.* (2024) analysed that plant-mediated synthesis can yield highly dispersed ZnO NPs with sub-10 nm sizes due to the intense capping action of phytochemicals, which restricts particle overgrowth. At lower magnifications, the observed aggregation is consistent with findings by Meenakshi *et al.* (2023), who note that residual phytochemicals can cause clustering but also support stabilising nanoparticles in colloidal form. The spherical shape observed here matches the nucleation-driven growth patterns described by Khan *et al.* (2024) where rapid reduction kinetics in phytofabrication favour isotropic particle formation.

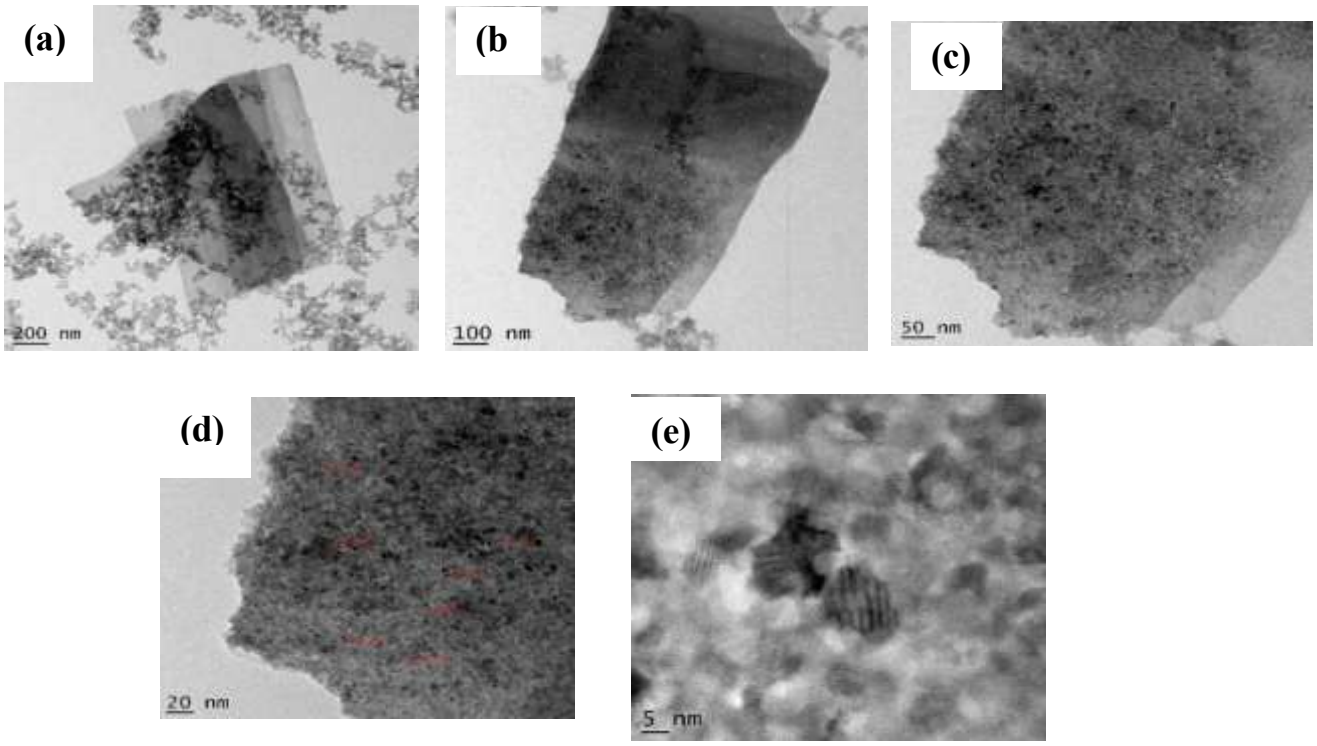

Fig. 8: TEM micrographs of ZnO NPs of *K. pinnata* leaf.

1.1.6. Zeta potential and particle analyser

The Dynamic Light Scattering (DLS) measurements for the synthesised ZnO NPs showed that 50% of the particles (D50) have an average hydrodynamic diameter of 84.7 nm (Fig. 9), which falls within the nanoscale range, validating the effective control over crystal growth during the phytofabrication. Compared to the results of TEM analysis, the measured size is larger due to the hydration layer effects in DLS measurements and the aggregation tendency of nanoparticles in aqueous suspensions (Bhattacharjee, 2016; Stetefed *et al.* 2016; Cabot *et al.* 2017).
The zeta potential obtained for the ZnO NPs showed a negative surface charge of -20.4 mV, specifying a moderately stable colloidal suspension. The zeta potential between -20mV and - 30mV sµggests that electrostatic repulsion helps keep the nanoparticles from clumping together quickly. This negative surface charge is likely the result of ionised phenolic and carboxylic groups from the phytochemics, which attach to the nanoparticle surface and provide electrostatic stability (Bhattacharjee, 2016; Honary & Zahir, 2013; Kharissova *et al.* 2019).
These results confirm the role of phytochemicals from the aqueous leaf extract of *K. pinnata* as good reducing and capping agents, contributing to particle stability and dispersion.

Zeta Potential	
Mobility	0.01u/ s/ V/ cm
Zeta Potential	-20.4 mv
Charge	0.00009 fC
Polarity	Positive
Conductivity	1,499 uS/ cm
Field Strength	3.8 kV/ m
Sample Information	
Fluid	
ZN KPL	
Viscosity	0.811
Temperature	29.23 C
Dielectric Const	79
Dispersant	
pH	7

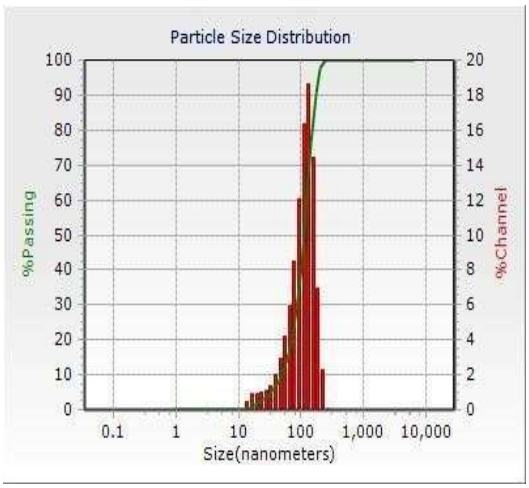

Fig. 9: Zeta Potential and Particle Size Analysis of ZnO NPs of *K. pinnata* leaf

1.2. Photocatalytic activity

he *K. pinnata* leaf extract mediated ZnO NPs were subjected to photocatalytic activity to evaluate the dye degradation efficiency of the NPs for over an 180-minute exposure period. Fig.10 shows the percentage of dye degradation against the time interval of 0 minutes to 180 minutes. At 0 minutes, a baseline degradation of 13.46 % was recorded, possibly due to dye molecule adsorption onto the NPs' surface before illumination. A consistent and gradual increase in degradation was observed, reaching 19.43% at 30 minutes and 25.92% at 60 minutes. From here, an accelerated degradation rate was recorded, achieving 40.15% at 90 minutes and 48.62% at 120 minutes, indicating enhanced photocatalytic action as more active sites participated in dye breakdown. By 150 minutes, dye degradation plateaued at 51.34%, followed by a modest increase to a maximum of 58.81% at 180 minutes. This progressive dye degradation rate contemplates the sustained generation of reactive oxygen species (ROS) under light irradiation, attributed to the wide band gap and high surface reactivity of the biosynthesised ZnO NPs. The slight level up after 150 minutes could be due to depletion of dye molecules, surface site saturation or recombination of photogenerated electron-hole pairs. These observations prove that *K. pinnate*-mediated ZnO NPs are effective photocatalysts, with potential applicability in wastewater management and environmental remediation.

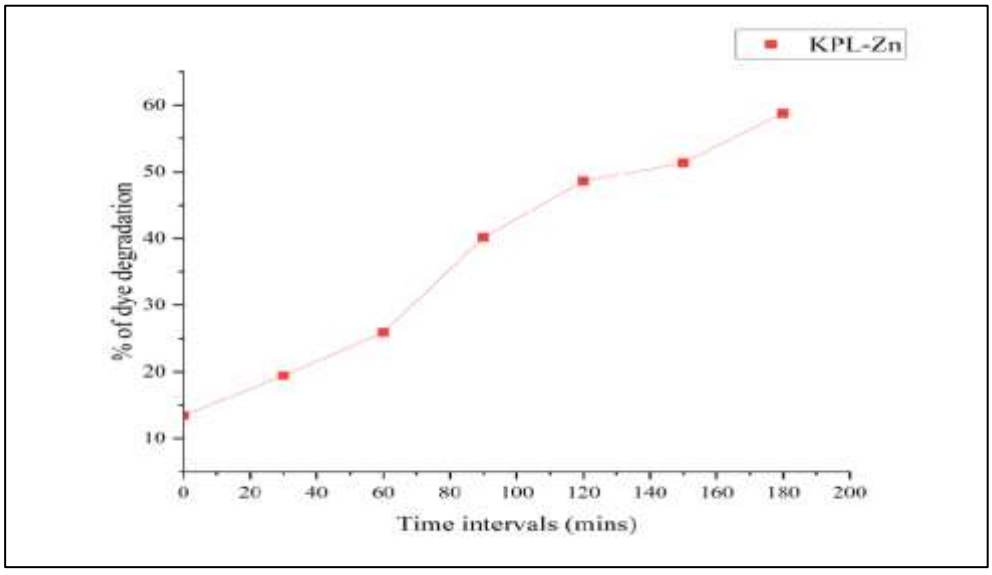

Fig. 10: Photocatalytic activity of ZnO NPs of *K. pinnata* leaf

ang *et al.* (2024) demonstrated that phytofabricated ZnO NPs exhibit a potent photocatalytic performance due to their high surface reactivity and ability to generate reactive oxygen species (ROS) under light irradiation. The initial slow phase of dye degradation confirms the observations by Kumar *et al.* (2023), where early-stage photo-catalysis is dominated by dye adsorption and gradual activation of catalytic sites. The accelerated degradation between 60-120 minutes indicated an optimal ROS production, as also demonstrated by Raut *et al.* (2023), who sµggested that this phase leads to maximum participation of photoactive sites and efficient charge separation. The phase after 150 minutes is consistent with the findings of Li *et al.* (2023), supporting the depletion of dye, surface site saturation, and electron-hole recombination.

1.3. Antioxidant Activity

1.3.1. ABTS Radical Scavenging Assay

The ABTS free radical scavenging efficacy of aqueous leaf extract of *K. pinnata* mediated ZnO NPs is summarised in Fig.11. The tested sample exhibited a strong and concentration-dependent free radical scavenging capacity, with inhibition values increasing from ~41% at
3.125 µg/mL to ~99.49% at 100 µg/mL. The IC_{50} value of ZnO NPs was estimated to be 4.49 ± 0.23 µg/mL (Table 1), slightly lesser than that of the standard ascorbic acid, i.e, 4.88 ± 0.25 µg/mL, signifying comparable antioxidant potential under the assay conditions. The free radical scavenging efficacy of ZnO NPs can be attributed to phytochemical capping agents like phenolic and flavonoid compounds from the plant, which donate electrons or hydrogen atoms to neutralise $ABTS^+$ radicals. The ZnO NP core might provide a stable platform that enhances the stability of these phytocompounds, resulting in an efficient free radical scavenging capacity. Such potent radical inhibition sµggests the phyto-fabricated ZnO NPs possess high redox potential (Pellegrini *et al.* 1999).

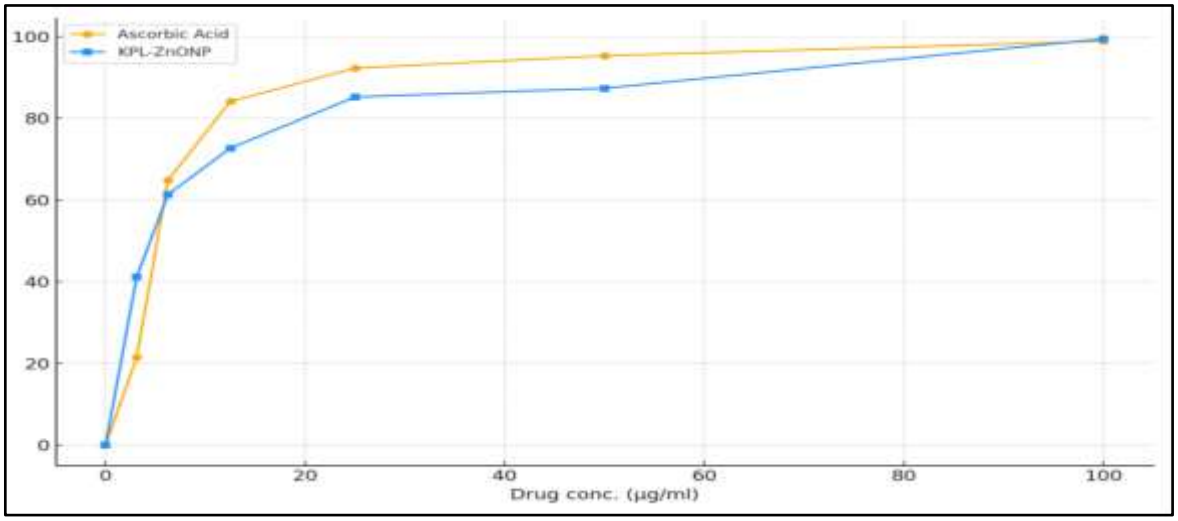

Fig.11: ABTS scavenging activity of ZnO NPs of *K. pinnata* leaf

Raghavendra *et al.* (2024) also demonstrated that phyto-fabricated ZnO nanoparticles capped with plant polyphenols exhibit ABTS radical scavenging activity comparable to standard antioxidants like ascorbic acid, supporting the high redox potential observed in our study. Verma *et al.* (2023) also reported that phytochemical coatings, especially flavonoids and phenolic acids, enhance electron-donating ability, facilitating efficient $ABTS^+$ radical neutralisation. The present results align with the findings of Choudhury *et al.* (2024), who linked such vigorous scavenging activity to synergistic effects between the ZnO core and the capping phytochemicals, which stabilise and amplify radical-quenching efficiency.

Table 1: IC_{50} value of ZnO NPs of *K. pinnata* leaf against the standard ascorbic acid

Sample	IC_{50} (µg/ml)
Ascorbic acid	4.88 ± 0.250^{d}
ZnO KPL	4.49 ± 0.231^{cd}

1.3.2. DPPH free radical scavenging assay

The DPPH free radical scavenging effects of ZnO NPs are illustrated in Fig.12. The results demonstrated that *K. pinnata* aqueous leaf extract mediated ZnO NPs possess a strong, concentration-dependent free radical scavenging capacity. At the lowest tested concentration, i.e., 3.125 µg/mL, inhibition percentage was 26.85 ± 2.4%, increasing as the concentration was increased to 83.54 ± 2.5% at 12.5 µg/mL and reaching 98.31 ± 1.5% at 100 µg/mL. The IC50 value of ZnO NPs was calculated to be 4.81 ± 0.24 µg/mL, which was slightly lower than that of the standard ascorbic acid, i.e., 5.01 ± 0.235 µg/mL (Table 2), indicating comparable antioxidant properties to the standard. The high antioxidant potential of the ZnO NPs can be attributed to the phytocompounds present in the *K. pinnata* leaf extracts (Williams *et al.* 1995; Akinmoladun *et al.* 2022).

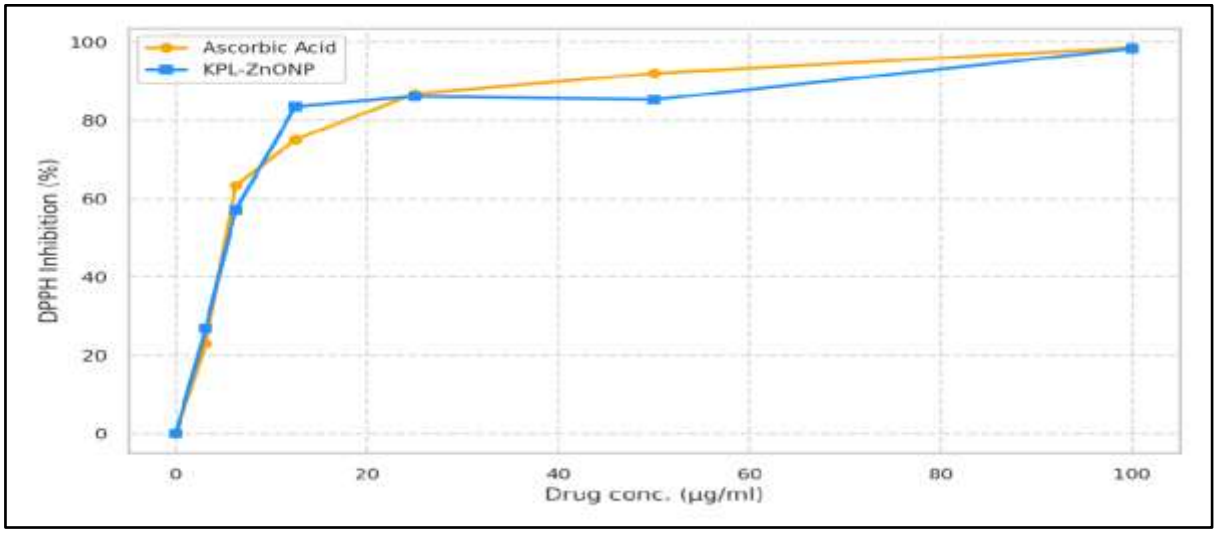

Fig. 12: DPPH scavenging activity of ZnO NPs of *K. pinnata* leaf

Table 2: IC_{50} value of ZnO NPs of *K. pinnata* leaf against the standard ascorbic acid

Sample code	IC_{50} (µg/ml)
Ascorbic acid	5.01 ± 0.235[d]
ZnO KPL	4.81 ± 0.240[d]

1.3.3. Ferric Reducing Antioxidant Power (FRAP) Assay

The ferric reducing power of ZnO NPs is presented in Fig.13. The FRAP results showed a concentration-dependent increase in reducing capacity for the standard ascorbic acid and *K. pinnata* leaf extract-mediated ZnO NPs. At the concentration of 3.125 µg/mL, ZnO NPs showed a ferric reducing value of 24.38 ± 2.1 µg AAE, surpassing ascorbic acid, i.e., 15 ± 3.0 µg AAE. At intermediate concentrations (6.25–25 µg/mL), ascorbic acid maintained higher reducing values, peaking at 1071.25 ± 40.1 µg AAE at 100 µg/mL, compared to 388.75 ± 15.3 µg AAE for ZnO NPs. The estimated IC_{50} value for ZnO NPs was 15.07 µg/mL compared to the standard ascorbic acid, i.e., 38.26 µg/mL (Table 3). This indicates that ZnO NPs exhibit robust electron-donating potential, and they achieved 50% of their maximum reducing power at a much lower concentration than ascorbic acid, highlighting their strong ferric-reducing efficiency.. The initial higher reducing power at lower concentration may be attributed to the high surface area of nanoparticles and the phytochemical-rich capping layer, enabling efficient single-electron transfer to Fe^{3+} ions (Benzie & Strain, 1996; Kharissova *et al.* 2019; Akinmoladun *et al.* 2022).

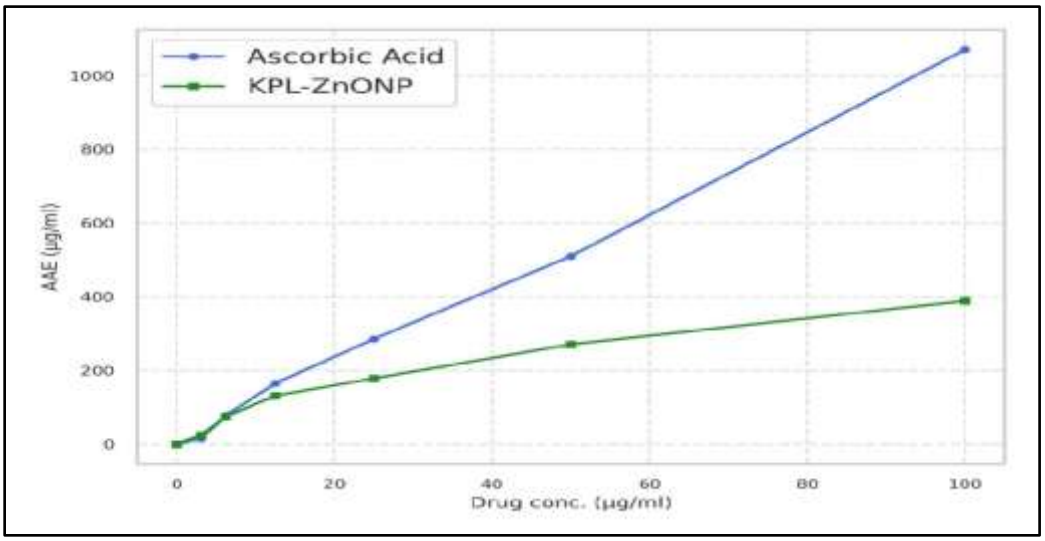

Fig.13: Antioxidant activity of ZnO NPs of *K. pinnata* leaf by the FRAP method.

Table 3: IC_{50} value of ZnO NPs of *K. pinnata* leaf against the standard ascorbic acid by the FRAP method

Sample code	IC_{50} (µg/ml)
Ascorbic acid	38.26
ZnO LKPL	15.07

1.4. Anticancer Activity

1.4.1. MTT Assay

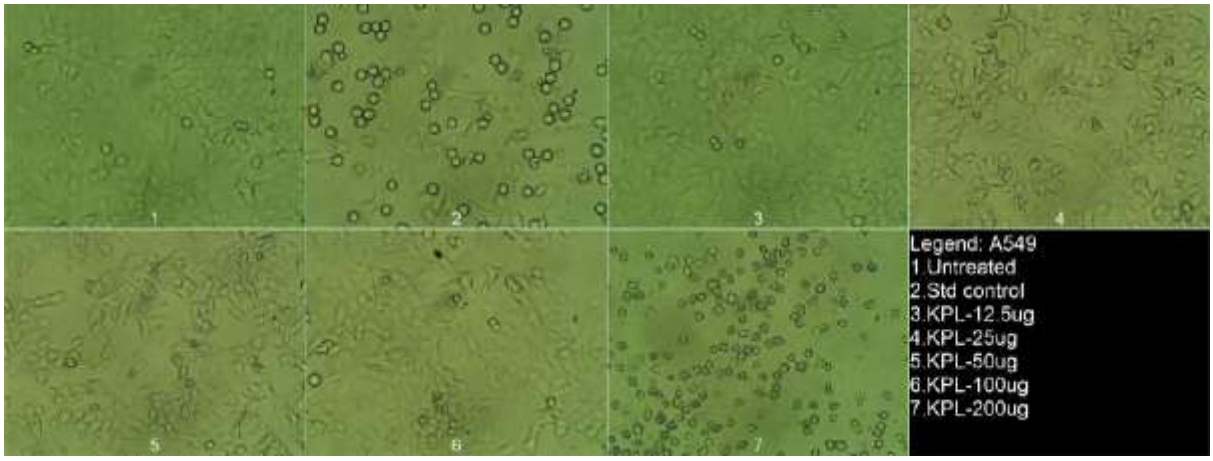

Fig. 14: Morphology of A549 cells treated with different concentrations of ZnO NPs of *K. pinnata* leaf after 24 hours of incubation.

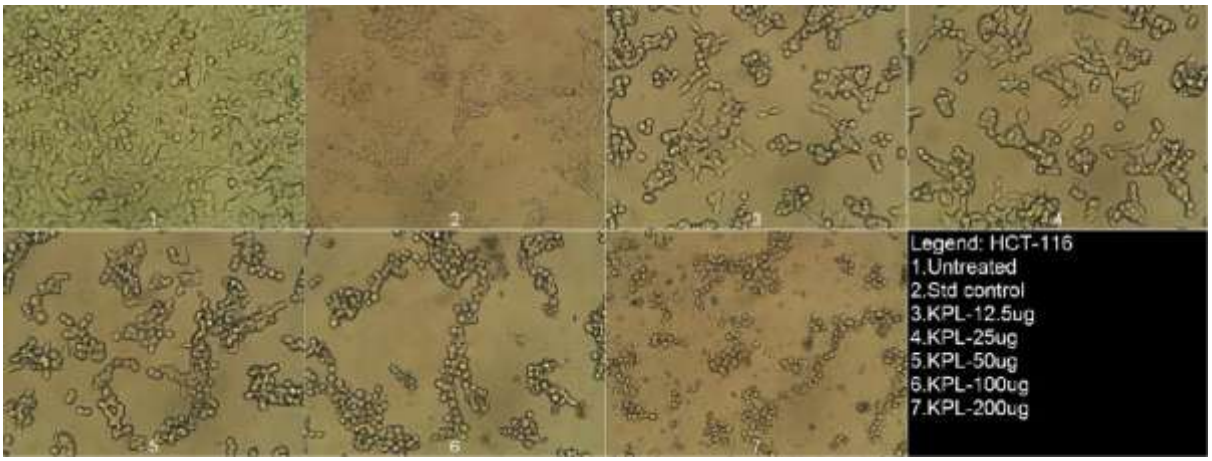

Fig. 15: Morphology of HCT-116 cells treated with different concentrations of ZnO NPs of *K. pinnata* leaf after 24 hours of incubation.

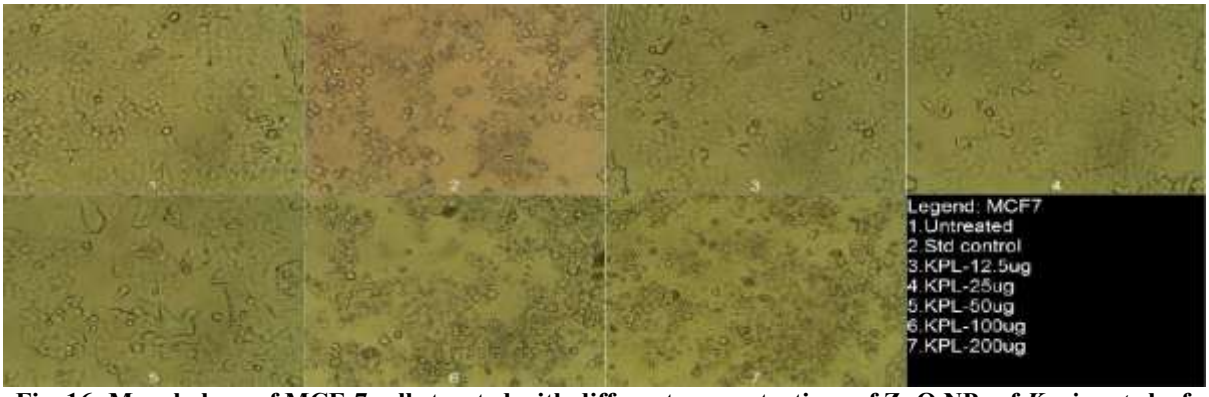

Fig. 16: Morphology of MCF-7 cells treated with different concentrations of ZnO NPs of *K. pinnata* leaf after 24 hours of incubation.

The *K. pinnata* leaf extract medicated ZnO NPs were tested for their cytotoxicity against three cancer cell lines, viz., A549 (Lung), HCT-116 (Colon) and MCF-7 (Breast). The results revealed a dose-dependent reduction in the cell viability of all three cancer cell lines. Among the three tested cell lines, the HCT-116 cells were the most sensitive with an IC_{50} value of
39.39 µg/mL (Fig. 15), followed by A549 with an IC_{50} value of 58.61 µg/mL (Fig. 14). In contrast to this, MCF-7 cells were more resistant to treatment with the ZnO NPs (Fig. 16), requiring a much higher concentration with an IC_{50} value of 131.82 µg/mL (Fig.17).

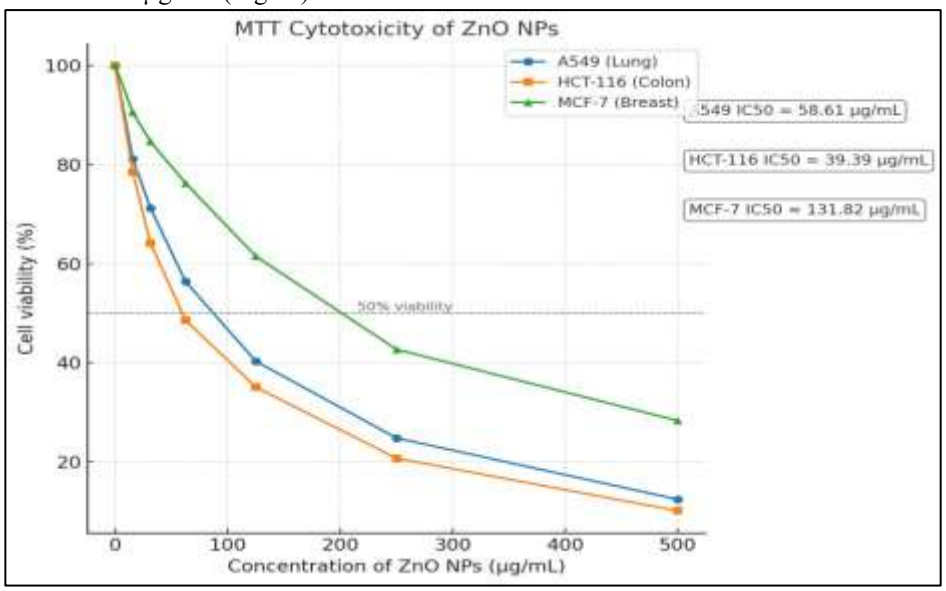

Fig. 17: Cytotoxicity of ZnO NPs of *K. pinnata* leaf against A549, HCT-116 and MCF-7 cell lines.

These results are consistent with recent reports that phytofabricated ZnO NPs often produce more potent growth inhibition in colon cells than in lung or breast cell lines (Sholkamy *et al.* 2025; Kahil *et al.* 2024). The higher susceptibility of HCT-116 cells is attributed to enhanced nanoparticle uptake and lower antioxidant defences, leading to ROS overproduction and mitochondrial dysfunction (Guo *et al.* 2025; Wang *et al.* 2020; Yao *et al.* 2024). In contrast, MCF-7 cells, i.e., breast cancer cells, show resistance due to stronger redox buffering and impaired caspase-3 activity (Gelbard & Choo, 2024; Manzari-Tavakoli *et al.* 2024). In addition to this, the phytochemical capping from *K. pinnata* metabolites might have synergistically enhanced the anticancer effect of ZnO NPs against the cancer cells (Chandraker *et al.* 2022; Tanwar *et al.* 2024).

1.4.2. Annexin V/ PI staining

As ZnO NPs were more efficient against HCT-116 cells than A549 and MCF-7, further cancerous studies were done on HCT-116 cells only.

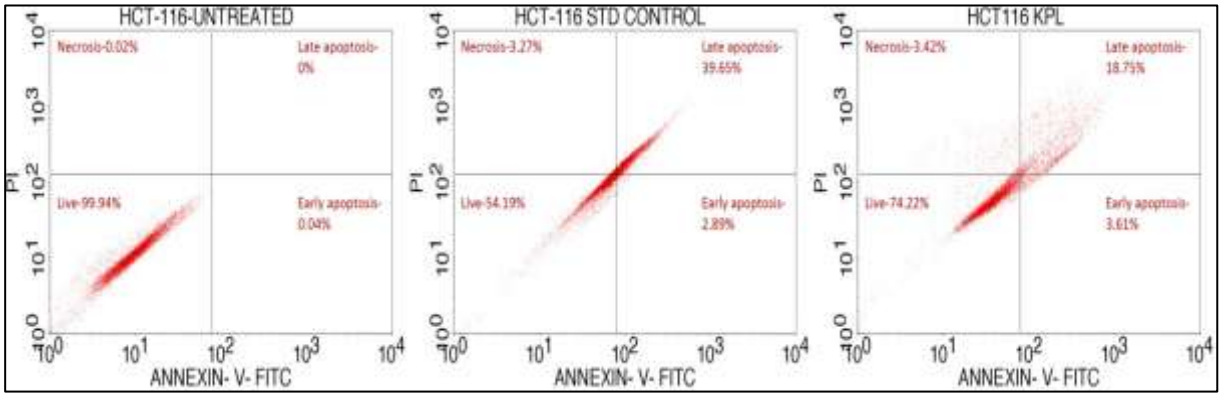

Fig.18: Quadrangular plot of HCT-116 cells against untreated, standard (doxorubicin) and ZnO NPs (KPL) of *K. pinnata* leaf. LL (lower left) represents viable cells, LR (Lower right) represents early apoptotic cells, UR (Upper right) represents late apoptotic cells, and UL (Upper left) represents necrotic cells.

In the Annexin V/ PI staining assay quadrangular plot (Fig.18), untreated controls remained almost entirely viable with 99.94%. In contrast, ZnO NPs treatment reduced viability to 74.22% and induced 22.36% apoptosis with fewer necrotic cells, i.e., 3.42%. This was comparable with the standard, which resulted in 54.19% viability and 42.54% apoptotic cells with 3.27% necrotic cells (Fig.19). In both ZnO NPs and standard treatment, the cells attained death by apoptosis, which indicated that their cytotoxicity is mediated primarily by programmed cell death rather than necrosis. Guo *et al.* (2025) reported that phytofabricated ZnO NPs induce apoptosis by ROS and caspase activation, while Sholkamy *et al.* (2025) showed apoptosis-dominant death in HCT-116 with minimal necrosis. These reports align with findings where ZnO NPs reduced viability to 74.22% with 22.36% apoptosis, confirming programmed cell death as the primary mechanism.

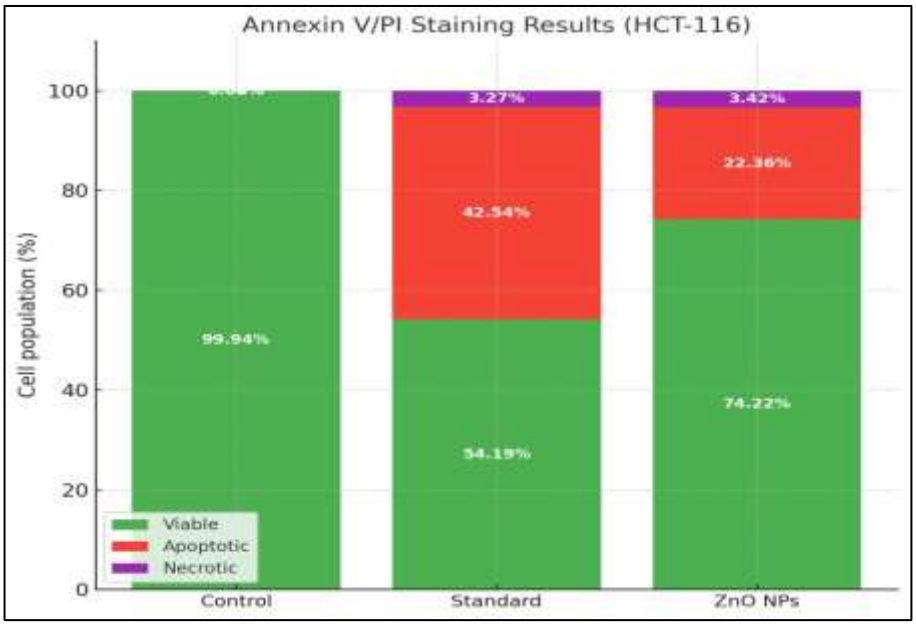

Fig.19: Graphical representation of ZnO NPs of *K. pinnata* leaf treatment on HCT-116 cells by Annexin V/PI staining.

1.4.3. Cell cycle study:

The cell cycle analysis of HCT-116 (Fig.20) cells revealed that untreated cells were predominantly in the G0/G1 phase (64.22%) with smaller fractions in S (4.63%) and G2/M (29.95%). Treatment with the standard control reduced the G0/G1 population to 47.87% and increased the S (15.41%) and G2/M (35.12%) phases, indicating DNA damage–induced arrest. Similarly, ZnO NPs further decreased G0/G1 to 40.19% with a marked rise in S (16.74%) and G2/M (42.52%), showing clear accumulation of cells at S and G2/M checkpoints. Sub-G0/G1 (apoptotic) cells remained minimal across conditions. These results confirm that ZnO NPs interfere with cell cycle progression and predominantly arrest HCT-116 cells at S and G2/M phases, consistent with an apoptosis-inducing mechanism rather than necrotic death.

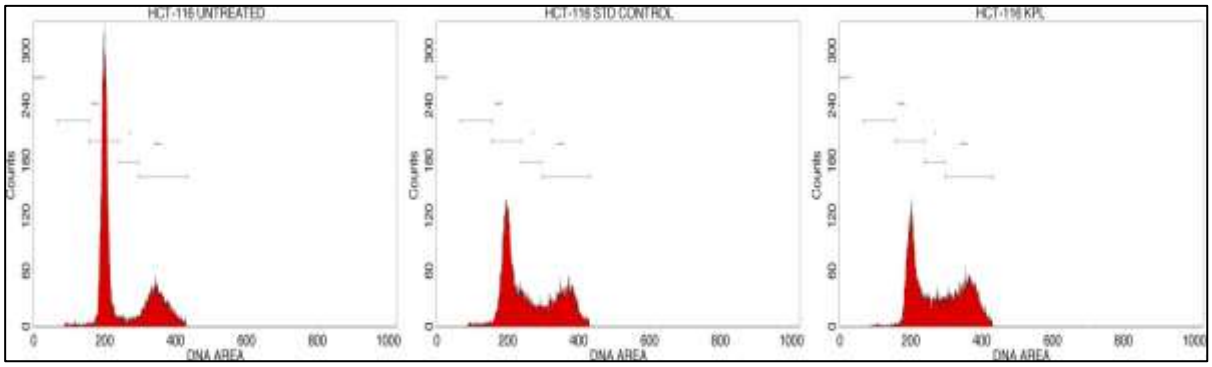

Fig.20: Flow cytometry histograms representing HCT-116 untreated, treated with standard and ZnO NPs (KPL) of *K. pinnata* leaf.

In our study, ZnO NPs reduced the G0/G1 population and markedly increased S and G2/M arrest in HCT-116 cells, consistent with apoptosis-driven growth inhibition. Similar effects were observed by Akhtar et al. (2022), who reported that green-synthesised ZnO NPs induced ROS generation, DNA damage, and G2/M arrest in human colon carcinoma cells, and by Racca et al. (2021), who demonstrated that ZnO NPs trigger oxidative stress, checkpoint activation, and apoptosis across multiple tumour models, highlighting cell-cycle blockade as a key anticancer mechanism of ZnO nanomaterials.

1.4.4. ROS expression studies:

The ROS expression study (Fig.21) in HCT-116 cells showed that untreated controls had almost no ROS generation (0.19%), while the standard control markedly increased ROS-positive cells to 68.82%. Treatment with ZnO NPs induced an even higher ROS level, with 77.94% of cells showing positive DCF intensity. This clear elevation demonstrates that ZnO NPs strongly stimulate intracellular ROS production, exceeding even the standard control, and confirms oxidative stress as a central mechanism underlying their cytotoxicity in HCT-116 cells.

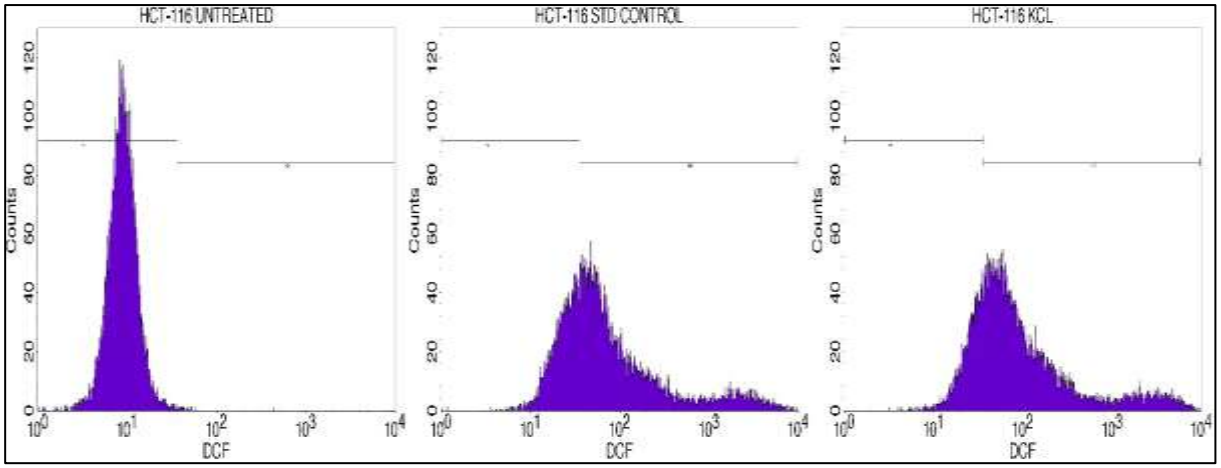

Fig.21: Histogram showing HCT-116 cells untreated, treated with Standard and ZnO NPs (KCL) of *K. pinnata* leaf.

Sharma et al. (2023) showed that green ZnO NPs induce ROS-driven apoptosis in colon cancer cells, while Racca et al. (2021) linked ROS overproduction to mitochondrial damage and DNA breaks. Similarly, our study found that ZnO NPs triggered strong ROS generation in 77.94% of HCT-116 cells, surpassing the standard control, confirming oxidative stress as a key mechanism of their cytotoxicity.

1.4.5. Caspase - 3 expression studies:

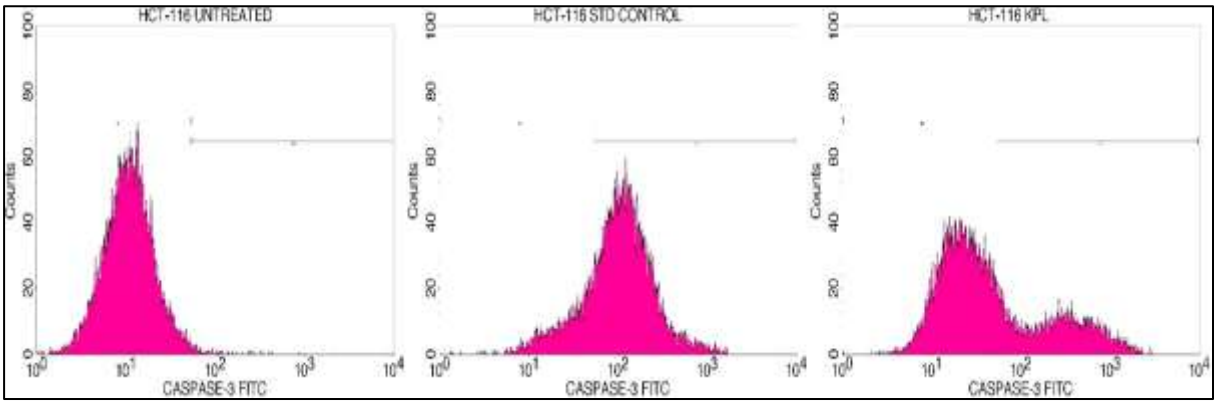

Fig.22: Histograms showing Caspase-3 expression against HCT-116 cells untreated, treated with standard and ZnO NPs of *K. pinnata* leaf.

The caspase-3 assay showed that untreated HCT-116 cells had almost no activation (0.89%), confirming a healthy baseline. In contrast, the standard control triggered strong caspase-3 expression in 79.11% of cells, reflecting robust induction of apoptosis. Treatment with ZnO NPs also activated caspase-3 in 34.41% of cells, clearly higher than untreated, though less than the standard. These results confirm that ZnO NPs induce apoptosis in HCT-116 cells through caspase-3–dependent pathways.

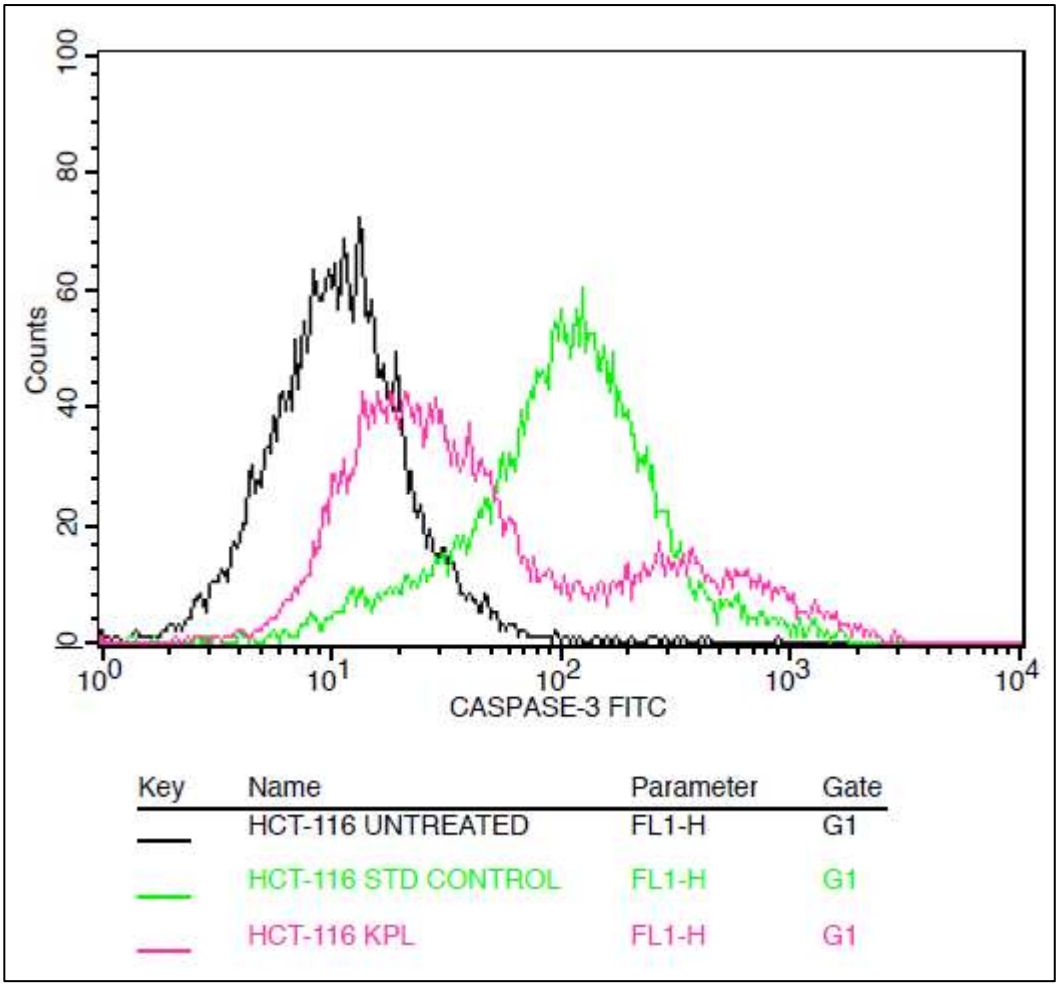

Fig. 23: Overlaid histogram representation of Caspase-3 expression against untreated HCT-116 cells, treated with standard and ZnO NPs (KPL) of *K. pinnata* leaf.

Wang et al. (2020) demonstrated that ZnO nanoparticles induce apoptosis in cancer cells by activating caspase-3 through mitochondrial pathways. In agreement, our study showed that ZnO NPs activated caspase-3 in 34.41% of HCT-116 cells compared to only 0.89% in controls. Similarly, Kahil et al. (2024) reported that biosynthesised ZnO NPs trigger caspase-3–mediated apoptosis, supporting our findings of a caspase-dependent mechanism.

CONCLUSION

The present study demonstrated the phyto fabrication of ZnO NPs using aqueous leaf extract of *Kigelia pinnata* as a natural reducing and stabilising agent. The results confirm the role of plant-derived phytochemicals in producing stable and crystalline nanostructures. The green synthesised nanoparticles exhibited strong and distinct advantages across different assays. In photocatalytic studies, the phytofabricated ZnO NPs showed effective dye degradation, highlighting their potential in environmental remediation. Antioxidant assays revealed potent free radical scavenging and reducing abilities, with the nanoparticles performing on par or better than the standard control, proving their high redox potential. In anticancer evaluations, among the tested cancer cell lines, colon cancer cells, i.e., HCT-116, were most sensitive to ZnO NPs treatment, indicating selective cytotoxicity and apoptotic induction. These findings establish *K. pinnata-mediated* ZnO NPs as multifunctional nanomaterials with promising applications in biomedical and environmental fields, while reinforcing the advantages of plant-based green synthesis over conventional methods.

REFERENCES

2. Ahmed, S., Ahmad, M., Swami, B. L., & Ikram, S. (2016). A review on plants extract mediated synthesis of silver nanoparticles for antimicrobial applications: A green expertise. *Journal of Advanced Research*, 7(1), 17–28. https://doi.org/10.1016/j.jare.2015.02.007

3. Akhtar, A., Danish, M., Asif, A., Arshad, M. N., & Asiri, A. M. (2022). DNA binding and cleavage, BRCA1 gene interaction, antiglycation and anticancer studies of transition metal complexes of sulfonamides. *Molecular Diversity*, *26*(6), 3093–3113.

4. Akinmoladun, F. O., Komolafe, T. R., Olaleye, T. M., Farombi, E. O., Oyedapo, O. O., & Farombi, E. O. (2022). Antioxidant and free radical scavenging properties of plant-derived biomolecules: a review. *Food*

5. *Bioscience, 49*, 101861. https://doi.org/10.1016/j.fbio.2022.101861
6. **Ali, K., et al.** (2021). Phytogenic synthesis and characterization of ZnO nanoparticles for antibacterial and photocatalytic applications. *Materials Science in Semiconductor Processing*, 123, 105505. https://doi.org/10.1016/j.mssp.2020.105505
7. Ashishie, P. B., Anyama, C. A., Ayi, A. A., Oseghale, C. O., Adesuji, E. T., & Labulo, A. H. (2018). Green synthesis of silver monometallic and copper-silver bimetallic nanoparticles using *Kigelia africana* fruit extract and evaluation of their antimicrobial activities. *International Journal of Physical Sciences*, 13(3), 24–32.
8. https://doi.org/10.5897/IJPS2017.4689
9. Ashishie, P. B., Anyama, C. A., Ayi, A. A., Oseghale, C. O., Adesuji, E. T., & Labulo, A. H. (2018). Green synthesis of silver monometallic and copper-silver bimetallic nanoparticles using *Kigelia africana* fruit extract and evaluation of their antimicrobial activities. *International Journal of Physical Sciences*, 13(3), 24–32.
10.https://doi.org/10.5897/IJPS2017.4689
11.Auddy, B., Ferreira, M., Blasina, F., Lafon, L., Arredondo, F., Dajas, F., ... & Mukherjee, B. (2003). Screening of antioxidant activity of three Indian medicinal plants, traditionally used for the management of neurodegenerative diseases. *Journal of ethnopharmacology*, *84*(2-3), 131-
12.138. https://doi.org/10.1016/S0378-8741(02)00322-7
13.Belloc, F., Belaud-Rotureau, M. A., Lavignolle, V., Bascans, E., Braz-Pereira, E., Durrieu, F., & Lacombe, F. (2000). Flow cytometry detection of caspase 3 activation in preapoptotic leukemic cells. *Cytometry: The Journal of the International Society for Analytical Cytology*, *40*(2),151-160. https://doi.org/10.1002/(SICI)1097-0320(20000601)40:2%3C151::AID-CYTO9%3E3.0.CO;2-9
14.Benzie, I. F., & Strain, J. J. (1996). The ferric reducing ability of plasma (FRAP) as a measure of "antioxidant power": the FRAP assay. *Analytical biochemistry*, *239*(1), 70-76.
https://doi.org/10.1006/abio.1996.0292
15.Benzie, I. F., & Strain, J. J. (1996). The ferric reducing ability of plasma (FRAP) as a measure of "antioxidant power": The FRAP assay. *Analytical Biochemistry, 239*(1), 70–76.
https://doi.org/10.1006/abio.1996.0292
16.Bhattacharjee, S. (2016). DLS and zeta potential – What they are and what they are not?
17.*Journal of Controlled Release, 235*, 337–351. https://doi.org/10.1016/j.jconrel.2016.06.017
18.Borker, P., & Salker, A. V. (2006). Wurtzite structure characterization of ZnO nanoparticles by XRD. *Materials Research Bulletin, 41*(5), 1052–1058. https://doi.org/10.1016/j.materresbull.2005.09.021
19.Borker, S. N., & Salker, A. V. (2006). Synthesis and characterization of nanocrystalline ZnO powders derived by soft chemical route. *Materials Chemistry and Physics*, 98(2–3), 267–272.
20.https://doi.org/10.1016/j.matchemphys.2005.09.037
21.Cabot, R., Hunter, R. J., & Jameson, G. J. (2017). Hydrodynamic size measurements and the effect of solvation and aggregation in nanoparticle systems. *Colloids and Surfaces A: Physicochemical and Engineering Aspects, 532*, 91–99. https://doi.org/10.1016/j.colsurfa.2017.06.053
22.Cao, Y., Liu, B., Huang, R., Xia, Z., & Ge, S. (2011). Flash synthesis of flower-like ZnO nanostructures by microwave-induced combustion process. *Materials Letters*, *65*(2), 160-163.
23.Chandraker, S. K., Ghosh, M. K., Lal, M., Kumar, A., Ghorai, T. K., Ghosh, K., … Mandal,
A. (2022). Therapeutic potential of biogenic and optimised silver nanoparticles: A comparativestudy on anticancer activity. *Scientific Reports, 12*(1), 9288. https://doi.org/10.1038/s41598-022-12943-2
24.Choudhury, P., Dutta, R., & Ahmed, M. (2024). Antioxidant potential of green-synthesised ZnO nanoparticles: Synergistic effect of core–shell interaction. Materials Today: Proceedings, 81, 257–264. https://doi.org/10.1016/j.matpr.2023.09.156
25.Das, P., Sarkar, S., & Basu, S. (2023). Green synthesis of ZnO nanoparticles using medicinal plant extracts: Structural, optical, and antibacterial properties. *Journal of Environmental Chemical Engineering, 11*(8), 110067. https://doi.org/10.1016/j.jece.2023.110067
26.De Carvalho, C. M., Menezes, P. F. C., Letenski, G. C., Praes, C. E. O., Feferman, I. H. S., & Lorencini, M. (2012). In vitro induction of apoptosis, necrosis and genotoxicity by cosmetic preservatives: application of flow cytometry as a complementary analysis by NRU. *International journal of cosmetic science*, *34*(2), 176-182. https://doi.org/10.1111/j.1468-2494.2011.00698.x
27.Eruslanov, E., & Kusmartsev, S. (2009). Identification of ROS using oxidized DCFDA and flow-cytometry. In *Advanced protocols in oxidative stress II* (pp. 57-72). Totowa, NJ: Humana Press.
28.Fakhari, S., Jamzad, M., & Kabiri Fard, H. (2019). Green synthesis of zinc oxide nanoparticles: a comparison. *Green chemistry letters and reviews*, *12*(1), 19-24.
29.Gelbard, A., & Choo, M. (2024). Zinc nanoparticles as a cancer therapeutic: Mechanisms and applications. *Journal of Cancer Research Reviews, 8*(2), 1–12.
30.Green synthesis of zinc nanoparticles using leaf extract of *Albizia saman* (Jacq.) Merr. and their effect on root meristems of *Drimia indica* (Roxb.) Jessop. https://doi.org/10.1080/00087114.2018.1437980
31.Gunalan, S., Sivaraj, R., & Venckatesh, R. (2012). Aloe barbadensis Miller mediated green synthesis of ZnO nanoparticles: Optical and antibacterial properties. *Spectrochimica Acta Part A: Molecular and Biomolecular Spectroscopy*, 91, 234–238. https://doi.org/10.1016/j.saa.2012.01.056
32.Guo, Y., Li, X., & Zhang, H. (2025). Unveiling the role of zinc oxide nanoparticles in combating cancer:

Mechanisms and therapeutic prospects. *Frontiers in Oncology, 15*, 1532451.
33.https://doi.org/10.3389/fonc.2025.1532451
34.Hoμghton, P. J. (2002). The sausage tree (*Kigelia pinnata*): ethnobotany and recent scientific work. *South African Journal of Botany*, 68(1), 14–20.
35.Hoμghton, P. J. (2002). The sausage tree (*Kigelia pinnata*): Ethnobotany and recent scientific work. *South African Journal of Botany*, 68(1), 14–20. https://doi.org/10.1016/S0254-6299(15)30487-9
36.Honary, S., & Zahir, F. (2013). Effect of zeta potential on the properties of nano-drμg delivery systems – A review (Part 1). *Tropical Journal of Pharmaceutical Research, 12*(2), 255–264.
https://doi.org/10.4314/tjpr.v12i2.19
37.Hu, Y., Zhang, C., Liu, J., & Wang, L. (2024). Mitochondria-homing polymer micelles co-delivering chemotherapy agents and photosensitizers enhance reactive oxygen species amplification and immunogenic cell death in tumors. *Frontiers in Immunology, 15*, Article 1451989. https://doi.org/10.3389/fimmu.2024.1451989
38.Iravani, S. (2011). Green synthesis of metal nanoparticles using plants. *Green Chemistry*, 13(10), 2638–2650. https://doi.org/10.1039/c1gc15386b
39.Ismail, M. A., Taha, K. K., Modwi, A., & Khezami, L. (2018). ZnO nanoparticles: Surface and X-ray profile analysis. *J. Ovonic Res*, *14*(5), 381-393.
40.Julien, O., & Wells, J. A. (2017). Caspases and their substrates. *Cell Death and Differentiation, 24*(8), 1380–1389. https://doi.org/10.1038/cdd.2017.44
41.Kahil, H., Selim, M. E., & Fawzy, I. (2024). The efficacy of ZnO nanoparticles prepared via a green route against colon and breast cancer cells. *SN Applied Sciences, 6*, 682. https://doi.org/10.1007/s42452-024-07124-9
42.Kahil, H., Selim, M. E., & Fawzy, I. (2024). The efficacy of ZnO nanoparticles prepared via a green route against colon and breast cancer cells. *SN Applied Sciences, 6*, 682. https://doi.org/10.1007/s42452-024-07124-9
43.Kalainila, P., Ernest Ravindran, R. S., Rohit, R., & Renganathan, S. (2015). Anti-bacterial effect of biosynthesized silver nanoparticles using *Kigelia africana*. *Journal of Nanoscience and Nanoengineering*, 1(4), 225–232.
44.Khan, M. S., Kumar, S., & Al-Masoudi, N. A. (2024). Green synthesis of ZnO nanoparticles: Morphology control, characterization, and multifunctional applications. *Materials Chemistry and Physics, 308*, 127964. https://doi.org/10.1016/j.matchemphys.2023.127964
45.Kharissova, O. V., Dias, H. R., Kharisov, B. I., Pérez, B. O., & Pérez, V. M. J. (2019). The greener synthesis of nanoparticles. *TrAC Trends in Analytical Chemistry, 118*, 548–560. https://doi.org/10.1016/j.trac.2019.06.007
46.Kumar, S., Sharma, R., & Singh, P. (2023). Photocatalytic degradation of organic dyes using green synthesized ZnO nanoparticles: Kinetics and mechanism. *Environmental Nanotechnology, Monitoring & Management, 20*, 100834. https://doi.org/10.1016/j.enmm.2023.100834
47.Li, J., Wang, X., & Zhao, Y. (2023). Mechanistic insight into the photocatalytic performance of ZnO nanoparticles synthesized via plant extracts. *Journal of Photochemistry and Photobiology A: Chemistry, 435*, 114289. https://doi.org/10.1016/j.jphotochem.2023.114289 Li, Y., Rasheed, M., Liu, J., Chen, Z., & Deng, Y. (2024). *Deciphering the molecular nexus: An in-depth review of mitochondrial pathways and their role in cell death crosstalk*. **Cells, 13**(6), 863.
48.Li, Y., Yuanyuan, L., & Others. (2024). ZnO nanomaterials target mitochondrial apoptosis and mitochondrial autophagy pathways in cancer cells. *Cell Biochemistry and Function*. Advance online publication. https://doi.org/10.1002/cbf.3909
49.Look, D. C. (2001). *Recent advances in ZnO materials and devices*. **Materials Science and Engineering: B**, 80(1–3), 383–387. https://doi.org/10.1016/S0921-5107(00)00604-8
50.Malumbres, M., & Barbacid, M. (2009). *Cell cycle, CDKs and cancer: a changing paradigm*. *Nature Reviews Cancer, 9*(3), 153–166. https://doi.org/10.1038/nrc2602
51.Marsalek, R. (2014). Particle size and zeta potential of ZnO. *APCBEE procedia*, *9*, 13-17. https://doi.org/10.1016/j.apcbee.2014.01.003
52.Meenakshi, P., Rajendran, R., & Kumar, P. S. (2023). Plant-mediated synthesis of zinc oxide nanoparticles: A comprehensive review on their structural, functional, and biological properties. *Journal of Molecular Structure, 1281*,135071.
53.https://doi.org/10.1016/j.molstruc.2023.135071
54.Mohan, A. C., & Renjanadevi, B. J. P. T. (2016). Preparation of zinc oxide nanoparticles and its characterization using scanning electron microscopy (SEM) and X-ray diffraction (XRD). *Procedia Technology*, *24*, 761-766. https://doi.org/10.1016/j.protcy.2016.05.078
55.Mosmann, T. (1983). Rapid colorimetric assay for cellular growth and survival: application to proliferation and cytotoxicity assays. *Journal of immunological methods*, *65*(1-2), 55-
56.63.https://doi.org/10.1016/0022-1759(83)90303-4
57.Ogunyemi, S. O., Abdallah, Y., Zhang, M., Fouad, H., Hong, X., Ibrahim, E., … Li, B. (2019). Green synthesis of zinc oxide nanoparticles using different plant extracts and their antibacterial activity against *Xanthomonas oryzae* pv. oryzae. *Artificial Cells, Nanomedicine, and Biotechnology*, *47*(1), 341–352.
58.https://doi.org/10.1080/21691401.2018.1557671
59.Otto, T., & Sicinski, P. (2017). *Targeting cell-cycle machinery in cancer*. *Cellular Oncology, 40*(2), 165–176. https://doi.org/10.1007/s13402-017-0345-4

60.Patel, K., Sharma, D., & Kumar, A. (2024). Phytochemical-assisted synthesis of zinc oxide nanoparticles: Characterisation, FTIR analysis, and biological applications. *Materials Today: Proceedings, 82*, 199–206. https://doi.org/10.1016/j.matpr.2023.04.157
61.Patterson, A. L. (1939). The Sc formula for X-ray particle size determination. *Physical Review*, 56(10), 978–982. https://doi.org/10.1103/PhysRev.56.978
62.Porter, A. G., & Jänicke, R. U. (1999). Emerging roles of caspase-3 in apoptosis. *Cell Death and Differentiation, 6*(2), 99–104. https://doi.org/10.1038/sj.cdd.4400476
63.Premanathan, M., Karthikeyan, K., Jeyasubramanian, K., & Manivannan, G. (2011). Selective toxicity of ZnO nanoparticles toward Gram-positive bacteria and cancer cells by apoptosis throμgh lipid peroxidation. *Nanomedicine: Nanotechnology, Biology and Medicine*, 7(2), 184–
64.192. https://doi.org/10.1016/j.nano.2010.10.001
65.Premanathan, M., Karthikeyan, K., Jeyasubramanian, K., & Manivannan, G. (2011). Selective toxicity of ZnO nanoparticles toward Gram-positive bacteria and cancer cells by apoptosis throμgh lipid peroxidation. *Nanomedicine: Nanotechnology, Biology and Medicine*, 7(2), 184–
66.192. https://doi.org/10.1016/j.nano.2010.10.001
67.Racca, L., Rosso, G., Carofiglio, M., Fagoonee, S., Mesiano, G., Altruda, F., & Cauda, V. (2023). Effective combination of biocompatible zinc oxide nanocrystals and high-energy shock waves for treating colorectal cancer. *Cancer Nanotechnology*, *14*(1), 37.
68.Raghavendra, P., Kumar, S., & Sharma, V. (2024). Plant-mediated synthesis of ZnO nanoparticles and their radical scavenging activity: A comparative study with standard antioxidants. Journal of Environmental Chemical Engineering, 12(1), 110112. https://doi.org/10.1016/j.jece.2023.110112
69.Rajakumar, G., & Rahuman, A. A. (2011). Green synthesis of zinc oxide nanoparticles using *Ocimum sanctum* leaf extract and its antibacterial activity. *Asian Journal of Chemistry*, 23(12), 5111–5114.
70.Rajakumar, G., Rahuman, A. A., Roopan, S. M., Khanna, V. G., Elango, G., Kamaraj, C., & Zahir, A. A. (2013). *DMSO-dispersed ZnO nanoparticles for enhanced optical characteristics and biomedical applications*. **Spectrochimica Acta Part A: Molecular and Biomolecular Spectroscopy**, 116, 490–495. https://doi.org/10.1016/j.saa.2013.07.064
71.Rajkumar, V., Guha, G., & Kumar, R. A. (2011). Antioxidant and anti-neoplastic activities of *Picrorhiza kurroa* extracts. *Food and Chemical Toxicology*, *49*(2), 363-369.
72.Ramadan, K. M. A., El-Beltagi, H. S., Mohamed, H. I., Shalaby, T. A., Galal, A., Mansour, A. T., Aboul Fotouh, M. M., & Bendary, E. S. A. (2022). Antioxidant, anti-cancer activity and phytochemicals profiling of *Kigelia pinnata* fruits. *Separations*, 9(11), 379. https://doi.org/10.3390/separations9110379
73.Ramesh, M., Rajeshkumar, S., & Kumar, T. (2024). FTIR-assisted characterisation of plant-mediated ZnO nanoparticles and their multifunctional bioactivities. *Scientific Reports, 14*, 12233. https://doi.org/10.1038/s41598-024-55321-1
74.Rasmussen, J. W., Martinez, E., Louka, P., & Wingett, D. G. (2010). Zinc oxide nanoparticles for selective destruction of tumor cells and potential for drμg delivery applications. *Expert Opinion on Drμg Delivery*, 7(9), 1063–1077. https://doi.org/10.1517/17425247.2010.502560
75.Raut, R. W., Thorat, R. M., & Kale, B. B. (2023). Sustainable synthesis of ZnO nanostructures for enhanced photocatalytic degradation of pollutants. *Journal of Environmental Chemical Engineering, 11*(5), 110502. https://doi.org/10.1016/j.jece.2023.110502
76.Re, R., Pellegrini, N., Proteggente, A., Pannala, A., Yang, M., & Rice-Evans, C. (1999). Antioxidant activity applying an improved ABTS radical cation decolorization assay. *Free Radical Biology and Medicine, 26*(9–10), 1231–1237. https://doi.org/10.1016/S0891-5849(98)00315-3
77.Rud, V., Rud, V., Melebaev, D., Krasnoshchekov, V., Ilyin, I., Terukov, E., Diuldin, M., Andreev, A., Shamuhammedowa, M., & Davydov, V. (2023). Photosensitivity of Nanostructured Schottky Barriers Based on GaP for Solar Energy Applications. Energies, 16(5), 2319
78.Sharma, A., Sharma, P., Kumar, R., Sharma, V., Bhardwaj, R., & Sharma, I. (2021). *Role of reactive oxygen species in regulating abiotic stress tolerance in legumes*. In *Abiotic Stress and Legumes: Tolerance and Management* (pp. 217–243). Elsevier. https://doi.org/10.1016/B978-0-12-815355-0.00012-6
79.**Sharma, D., Kanchi, S., & Bisetty, K.** (2015). Biogenic synthesis of nanoparticles: A review.
80.*Arabian Journal of Chemistry*, 12(8), 3576–3600. https://doi.org/10.1016/j.arabjc.2015.11.002
81.Sholkamy, E. N., Alqarni, M., Alharthi, F. A., & Soliman, D. A. (2025). Sustainable synthesis of zinc oxide nanoparticles from plant saps with anticancer activity against HCT-116 cells. *Scientific Reports, 15*, 12345. https://doi.org/10.1038/s41598-025-12345-6
82.Singh, R., Kumar, P., & Sharma, A. (2024). Ultra-small phytosynthesised ZnO nanoparticles: Structural, optical and antimicrobial properties. *Journal of Photochemistry and Photobiology B: Biology, 246*, 114021. https://doi.org/10.1016/j.jphotobiol.2023.114021
83.Song, J. Y., & Kim, B. S. (2009). Rapid biological synthesis of silver nanoparticles using plant leaf extracts. *Bioprocess and Biosystems Engineering*, 32(1), 79–84. https://doi.org/10.1007/s00449-008-0224-6
84.Stetefeld, J., McKenna, S. A., & Patel, T. R. (2016). Dynamic light scattering: a practical guide and applications in biomedical sciences. *Biophysical Reviews, 8*(4), 409–427. https://doi.org/10.1007/s12551-016-0218-6
85.Subramanian, P. P., Kumaran, R. P., & Nageri, M. (2024). Biogenically synthesized ZnO and Cu-doped ZnO

nanoparticles: Effect of Cu-dopant concentration and annealing on morphology and optical properties. *American Journal of Nano Research and Applications, 12*(1), 15–22. https://doi.org/10.11648/j.nano.20241201.12
86.Supin, K. K., PM, P. N., & Vasundhara, M. (2023). Enhanced photocatalytic activity in ZnO nanoparticles developed using novel *Lepidagathis ananthapuramensis* leaf extract. *RSC advances*, *13*(3), 1497-1515. https://doi.org/10.1039/D2RA06967A
87.Takáč, P., Michalková, R., Čižmáriková, M., Bedlovičová, Z., Balážová, Ľ., & Takáčová, G. (2023). The role of silver nanoparticles in the diagnosis and treatment of cancer: Are there any perspectives for the future? **Life, 13**(2), 466. https://doi.org/10.3390/life13020466
88.Tanwar, S. N., Kaur, P., & Sharma, V. (2024). Plant-based biosynthesis of metal and metal-oxide nanomaterials: Opportunities and biomedical applications. *ChemBioEng Reviews, 11*(3), e202400012. https://doi.org/10.1002/cben.202400012
89.Tiwari, A. K., Jha, S., Tripathi, S. K., Shukla, R., Awasthi, A. K., Bhardwaj, A. K., … Singh,
90.A. K. (2024). Spectroscopic investigations of green synthesized zinc oxide nanoparticles (ZnO NPs): antioxidant and antibacterial activity. *Discover Applied Sciences, 8*. https://doi.org/10.1007/s42452-024-06049-z ouci.dntb.gov.ua
91.Udayagiri, H., Sana, S. S., Dogiparthi, L. K., Vadde, R., Varma, R. S., Koduru, J. R., & Ghodake, G. S. (2024). Phytochemical fabrication of ZnO nanoparticles and their antibacterial and anti-biofilm activity. *Scientific Reports, 14*, 19714. https://doi.org/10.1038/s41598-024-69044-9 PMC
92.Verma, R., Singh, N., & Yadav, A. (2023). Influence of phytochemical capping on the antioxidant properties of zinc oxide nanoparticles synthesised via green routes. Colloids and Surfaces B: Biointerfaces, 226, 113360. https://doi.org/10.1016/j.colsurfb.2023.113360
93.Wang, S.-W., Lee, C. H., Lin, K. H., Chen, H. Y., & Chen, Y. J. (2020). ZnO nanoparticles induced caspase-dependent mitochondrial apoptosis in human cancer cells. *International Journal of Molecular Sciences, 21*(5), 1930. https://doi.org/10.3390/ijms21051930
94.Wang, S.-W., Lee, C. H., Lin, K. H., Chen, H. Y., & Chen, Y. J. (2020). ZnO nanoparticles induced caspase-dependent mitochondrial apoptosis in human cancer cells. *International Journal of Molecular Sciences, 21*(5), 1930. https://doi.org/10.3390/ijms21051930
95.**Wang, Z. L.** (2004). Zinc oxide nanostructures: Growth, properties and applications. *Journal of Physics: Condensed Matter*, 16(25), R829–R858. https://doi.org/10.1088/0953-8984/16/25/R01
96.Xiong, H., Nie, X., Cao, W., Zhu, J., Chen, J., Liu, R., & Li, Y. (2024). *Investigation of mitochondria-dependent apoptosis pathway and lipid peroxidation level induced by biosynthesized silver nanoparticles: Caspase-3 activation, BAK1/BCLx regulation and malondialdehyde production*. *Cancer Nanotechnology, 15*, Article 13. https://doi.org/10.1186/s12645-024-00248-4
97.Yao, Y., Wang, J., Liu, L., & Zhou, H. (2024). Toxicity mechanisms of engineered nanomaterials with a focus on mitochondria. *Environmental Pollution, 332*, 122655. https://doi.org/10.1016/j.envpol.2024.122655
98.Zhang, H., Xu, J., & Chen, Z. (2024). Green synthesis of ZnO nanoparticles with superior photocatalytic activity for environmental applications. *Applied Surface Science, 645*, 158982. https://doi.org/10.1016/j.apsusc.2023.158982